VIRTUAL GAMMA CAMERA FOR EDUCATIONAL PURPOSES

139082

by

Ozan Yılmaz

B.S. in Electrical Engineering, İstanbul Technical University, 2000

Submitted to the institute of Biomedical Engineering

in partial fulfillment of the requirements

for the degree of

Master of Science

in

Biomedical Engineering
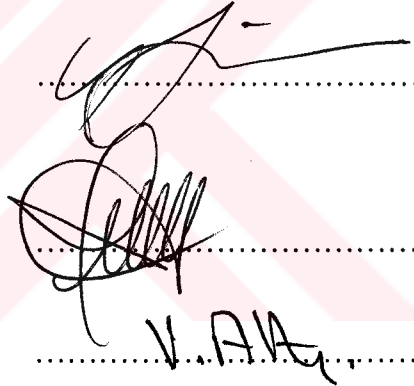
Boğaziçi University
June, 2003

VIRTUAL GAMMA CAMERA FOR EDUCATIONAL PURPOSES

APPROVED BY:

Doç. Dr. Albert Güveniş ....
(Thesis Supervisor)

Prof.Dr. Yekta Ülgen ....

Prof.Dr. Vural Altın ....

DATE OF APPROVAL: June 17, 2003

ACKNOWLEDGMENTS

I would like to thank my thesis supervisor Assoc. Prof. Albert Güveniş for his patience, tolerance, and academic support during my study. I would also like to thank Assoc. Prof Michael Ljungberg who helped me in getting through Monte Carlo simulation problems.

Also many thanks to my family and my friends Çelik Özdemir, Devrim Özkan, Aslı Bal, Emrah Duruer for their supports.

ABSTRACT

VIRTUAL GAMMA CAMERA FOR EDUCATIONAL PURPOSES

Nuclear medicine is a medical specialty that uses painless, safe, and cost-effective techniques to image the body and treat disease. In nuclear medicine, very small amounts of radioactive materials or radiopharmaceuticals are used to diagnose and treat diseases. The radiopharmaceuticals that are attracted to specific organs, bones, or tissues, emit gamma rays that can be detected by gamma or PET cameras. These cameras work with computers to form images, which provide data and information about the imaged area of body. The importance of Monte Carlo simulation in nuclear medicine imaging is increased by recent developments in nuclear medicine instrumentation and processing systems. The Monte Carlo method is very useful in medical physics due to the stochastic nature of radiation emission, transport and detection processes. Some of the applications of the Monte Carlo method in nuclear medical imaging are: Detector modeling, pharmacokinetic modeling, imaging systems and collimators design, attenuation and scatter correction techniques, image reconstruction algorithms, dosimetry and treatment planning. The aim of this work is to design a user-friendly interface that can perform a gamma camera simulation by using the Monte Carlo method. The purpose of this interface is to give the opportunity to students and researchers who have basic knowledge about gamma cameras, to understand the fundamentals of gamma camera imaging and to study the effects of the camera characteristics and parameters on the simulated images.

Keywords: Nuclear medicine, Monte Carlo simulations, gamma camera imaging, image quality

ÖZET

EĞİTİM AMAÇLI SANAL GAMA KAMERA

Nükleer tıp, vucüt görüntülenmesi ve hastalıkların tedavisinde güvenli, acısız ve ekonomik teknikler kullanan bir uzmanlık alanıdır. Nükleer tıpta, hastalığın teşhis ve tedavisi için çok küçük miktarlarda radyoaktif materyaller kullanılır. Nükleer tıpta kullanılan radyoaktif materyaller, özel tip kameralar (gama veya PET kameraları) tarafından dışardan izlenebilecek gama ışınları yayarlar. Bu kameralar bilgisayarlarla birlikte çalışarak vücüdun görüntülenen bölümüyle ilgili veri sağlayacak görüntü oluşturmak için kullanılırlar. Son yıllarda nükleer tıp aygıtlarındaki ve bilgisayar sistemlerindeki gelişmeler Monte Carlo yöntemi kullanılarak simülasyonun nükleer tıp görüntülemedeki önemini arttırmıştır. Yöntem, bilgisayar kodları kullanılarak deterministik yöntemlerle modellenemeyecek veya deneysel ölçümlerin yapılmasının uygulanamaz olduğu kompleks problemlerin çözümünde çok kullanışlıdır. Nükleer tıpta Monte Carlo yönteminin bazı uygulamaları şunlardır: Dedektör modellemesi, görüntüleme sistemleri ve kolimatör tasarımı, görüntü rekonstrüksiyon algoritmaları, atenüasyon ve saçılma düzeltme teknikleri, farmakokinetik modelleme. Bu çalışmada yapılmak istenen, Monte Carlo yöntemi temel alınarak yazılmış bilgisayar kodları kullanılarak eğitim amaçlı gama kamera simülasyonu gerçekleştirebilecek bir arayüzün tasarlanmasıdır. Bu sayede kullanıcı gama kamera karakteristik özelliklerinin ve çeşitli parametrelerin oluşturulan imaj üzerindeki etkisi benzetilebilecektir ve gama kameranın temellerini öğrenebilecektir.

Anahtar sözcükler: Nükleer tıpta görüntüleme, Monte Carlo yöntemi, gama kamera, imaj kalitesi.

TABLE OF CONTENTS

LIST OF FIGURES

LIST OF TABLES

LIST OF SYMBOLS

h	Planks constant
θ	Scattering angle
Z	Atomic number
hv	Photon energy
m_o	rest mass of the electron
c	Speed of light
μ	Linear attenuation coefficient
ρ	Density

LIST OF ABBREVIATIONS

FOV	Field of view
PMT	Photomultiplier tube
CRT	Cathode ray tube
PHA	Pulse Height Analyzer
CRT	Cathode Ray Tube
PET	Positron Emission Tomography
SPECT	Single-Photon Emission Tomography
FWHM	Full Width at Half Maximum
SG	Simple geometry
SB	Shape-based
VB	Voxel-based

1. INTRODUCTION

Nuclear medicine is a medical specialty that uses safe, painless, and cost-effective techniques both to image the body and treat disease. Nuclear medicine imaging is unique in that it documents organ function and structure, in contrast to diagnostic radiology, which is based upon anatomy. It is a way to gather medical information that may otherwise be unavailable, require surgery, or necessitate more expensive diagnostic tests [1][2][3].

Nuclear medicine uses very small amounts of radioactive materials or radiopharmaceuticals to diagnose and treat disease. Radiopharmaceuticals are substances that are attracted to specific organs, bones, or tissues. The radiopharmaceuticals used in nuclear medicine emit gamma rays that can be detected externally by gamma or PET cameras. These cameras work in conjunction with computers used to form images that provide data and information about the area of body being imaged [4][5].

The Monte Carlo method is widely used for solving problems involving statistical processes and is very useful in medical physics due to the stochastic nature of radiation emission, transport and detection processes. The method is very useful for complex problems that cannot be modeled by computer codes using deterministic methods or when experimental measurements may be impractical [6][7].

Several factors affect the image quality and the accuracy of the data obtained from a nuclear medicine scan. These include the physical properties of the detectors, collimator and gantry design, attenuation and scatter compensation and reconstruction algorithms [8]. Recent developments in nuclear medicine instrumentation and computer systems have increased the importance Monte Carlo simulation in nuclear medicine imaging. Monte Carlo methods can be used to optimize the design of imaging systems and to improve the quality and quantitative accuracy of reconstructed images [9].

Some of the applications of the Monte Carlo method in nuclear medical imaging are detector modeling, imaging systems and collimators design, image reconstruction algorithms, attenuation and scatter correction techniques, dosimetry and treatment planning, pharmacokinetic modeling [10].

The aim of this study is to design a user-friendly interface that can perform a gamma camera simulation by using Monte Carlo codes that are used in the field of nuclear imaging. Generally, simulation studies have several advantages over experimental studies. For any given model, it is very easy to change different parameters and investigate the effect of these changes on the performance of the system under investigation. The purpose of this interface is to give the opportunity, to students and researchers, who have basic knowledge about gamma camera, to understand the fundamentals of gamma camera imaging. The user will be able to study the effects of the camera characteristics and parameters on the simulated image, and understand trade-offs that must be considered for gamma camera imaging in front of a computer.

1.1   Thesis Outline

Chapter 1 is an introduction, outlining the study.

Chapter 2 provides information about physics of nuclear medicine.

Chapter 3 describes the gamma camera.

Chapter 4 presents detailed information about the gamma camera characteristics and image quality.

In Chapter 5, a detailed description of the general principles of the Monte Carlo method, and applications of Monte Carlo method in nuclear medical imaging is investigated.

In Chapter 6 design of the interface is described and program features are explained.

The conclusions, and recommendations for future work are presented in Chapter 7.

Appendix A includes sample experiments performed by the designed program and the results of the experiments. The user manual is presented in Appendix B. Appendix C includes the experiment handout. The source code of the program is given in Appendix D.

2. PHYSICS OF NUCLEAR MEDICINE

2.1 Radioactivity

Radioactivity is the spontaneous emission of charged particles or photons by an atomic nucleus that is in an unstable configuration. The nucleus is transformed to a more energetically stable form by this process. This event is called nuclear transformation, decay, or disintegration. Each decay event involves loss of mass or charge. The excess in energy is emitted either as an alpha particle (a helium nucleus), a beta particle (an electron) or as electromagnetic radiation (photons). The frequency (υ) of the photon and Planck's constant (h=6.626 10^{-34} Js) determines its energy. The unit of radioactivity is Curie, which is the quantity of a radioactive material having 3.7 10^{10} disintegrations per second [1].

A nucleus can also be transformed by electron capture, EC, where an orbital electron, usually from the K-shell, is acquired. The energy excess is emitted as gamma rays. In some cases, the nucleus is not de-excitated promptly after the transformation. Instead, it stays in an excited state, which is designated as a meta-stable state. This process is called isomeric transition, IT. The energy excess can also be transferred directly to an orbital electron, which will then be ejected from the atom. This process is called internal conversion, IC. The electrons in the K-shell are the most probable to be ejected. A vacancy in the electron shell will occur by electron capture and internal conversion transitions. This vacancy will rapidly be filled by an electron from the L-shell, and so on, with the emission of characteristic X-ray photons or Auger electrons [11].

Studies of the localization of administered radiopharmaceuticals by detection of the radiation from the radionuclides are part of nuclear medicine imaging. The radiopharmaceuticals can be administered to the patient by injection, orally or by inhalation. A radiopharmaceutical consists of a radionuclide with suitable radiation characteristics, which is usually labeled in a chemical reaction to a carrier. Then the physiological and biological behavior of the carrier can be traced.

Using radionuclides as tracers for *in vivo* studies is very useful. The physiological behavior and the metabolism in different organs can be studied. Also detection of lesions can be achieved. Tc-99m, the most commonly used radionuclide in nuclear medicine, decays to its normal ground state with a half-life of 6.03 h by primarily emitting a gamma ray at 140.05 keV (which is easily detectable) and has been incorporated into a variety of radiopharmaceuticals to tag specific biochemical functions *in vivo* in virtually every human organ [1].

Table2.1
Important radionuclides used in nuclear medicine [11].

Radionuclide	Decay	Half-life	Principal energy
^{57}Co	EC	271.6 days	122 keV
			137 keV
^{67}Ga	EC	78.2 hours	93 keV
			185 keV
$^{99}Tc^m$	IT	6.02 hours	140 keV
^{111}In	IC	2.83 days	171 keV
			245 keV
$^{113}In^m$	IT	1.66 hours	392 keV
^{123}I	EC	13.02 hours	159 keV
^{125}I	EC	60.2 days	35.5 keV
^{131}I	β^-	8.06 days	364 keV
^{133}Xn	β^-	5.3 days	81 keV
^{201}Tl	EC	73.5 hours	70-82 keV
			135 keV

Early devices used for photon imaging were based on scintillation detectors, which were mechanically scanned in a rectilinear pattern across a region of the patient. An important development was the scintillation camera, first presented by Anger in 1957 and later described in the literature [12]. The main difference between a scintillation camera and a rectilinear scanner is that in the former a large field-of-view scintillator is used which covers a large portion of the patient, instead of a small detector, which is scanned over the patient.

There are two types of scintigraphic studies: static studies and dynamic studies. In static studies the objective is to image a region of the patient after the administration of the radiopharmaceutical. In dynamic studies a small concentrated volume of the radiopharmaceutical (a bolus injection) is administered and then consecutive images are acquired over a period of time.

2.2   The Interactions of Photons with Matter

When electromagnetic radiation passes through matter, some photons will be totally absorbed by depositing its energy, some will penetrate the matter without interaction and some will interact and be scattered in different directions, with or without loosing energy. A photon interacts with the surrounding matter by four main interaction processes. The probability for each process depends on the photon energy and the atomic number, Z, of the material [2].
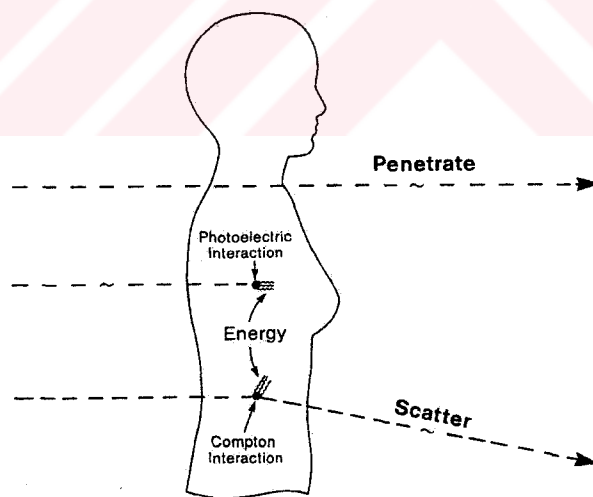
Figure 2.1 Photons entering the human body will penetrate, be absorbed, or produce scattered radiation [2].

2.2.1 Photoelectric Interaction

When a photoelectric interaction occurs, the energy of the photon is completely transferred to an atomic electron. The electron may thus gain sufficient kinetic energy to be ejected from the electron shell and begins to pass through the surrounding matter. The electron rapidly loses its energy and moves only a relatively short distance from its original location. The photon's energy is deposited in the matter close to the site of the photoelectric interaction. The energy transfer is a two-step process. The photoelectric in which the photon transfers its energy to the electron is the first step. The depositing of the energy in the surrounding matter by the electron is the second step.
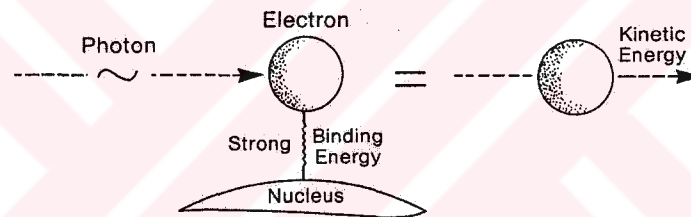
Figure 2.2 Photoelectric interaction [2].

The energy of the incoming photon must be higher that the binding energy for the electron. If the binding energy is more than the energy of the photon, a photoelectric interaction cannot occur. The most probable location for the photoelectric interaction is with the most tightly bounded electrons in the K-shell. A photoelectric interaction results in a vacancy in the atomic electron shell which, however, will be rapidly filled by an electron from one of the outer electron shells. The difference in binding energy between the two electron shells can be emitted either as a characteristic X-ray photon or as one or several Auger electrons. The relative probability for the emission of a characteristic X-ray photon is given by the fluorescence yield w. Characteristic X-ray emission is more probable for high-Z materials.

The cross-section for a photoelectric interaction depends strongly on the photon energy and the atomic number, Z, of the material and can be described approximately by

$$\tau_{photo} \cong \frac{Z^5}{(h\nu)^{3.5}}$$
(2.1)

2.2.2 Incoherent Scattering

In this process, the photon interacts with an atomic electron and is scattered through an angle θ relative to its incoming direction. Only a fraction of the photon energy is transferred to the electron. After incoherent scattering (or Compton scattering), the scattered photon energy $h\nu'$ is given by

$$h\nu' = \frac{h\nu}{1 + \frac{h\nu}{m_0 c^2}(1 - \cos\theta)}$$
(2.2)

where m_0 is the rest mass of the electron and c is the speed of light. Equation 2.2 is derived on the assumption that an elastic collision occurs between the photon and an electron, and that the electron is initially free and at rest. It is evident from equation 2.2 that the maximum energy transfer takes place when the photon is back-scattered 180° relative to its incoming direction and that the relative energy transfer from the photon to the electron increases for increasing photon energies. The differential cross-section per electron for an incoherent scattering of unpolarized photons, derived by Klein and Nishina, can be calculated from

$$\frac{d\sigma^e_{KN}}{d\Omega} = \frac{r_e^2}{2}\left[\frac{h\nu'}{h\nu}\right]^2\left[\frac{h\nu}{h\nu'} + \frac{h\nu'}{h\nu} - \sin^2\theta\right]$$
(2.3)

where

$$r_e = \frac{e^2}{4\pi\varepsilon_0 m_0 c^2}$$
(2.4)

is the classical electron radius. Equation 2.3 has been derived assuming that the interacting electron is free and at rest. The differential cross-section per atom can be calculated by multiplying the Klein-Nishina cross-section by the number of electrons Z in order to take into account the fact that atomic electrons are energetically bound to the nucleus. The Klein-Nishina cross-section per electron should be multiplied by the incoherent scattering function $S(x,Z)$ i.e.

$$\frac{d\sigma^a{}_{incoh}}{d\Omega} = \frac{d\sigma^e{}_{KN}}{d\Omega} S(x,Z) \qquad (2.5)$$

where $x = \sin(\theta/2)\lambda$ is the momentum transfer parameter and A, is the photon wavelength. For high-energy photons, the function $S(x,Z)$ approaches the atomic number Z and the cross-section will thus approach the Klein-Nishina (Evans) [13] cross-section.
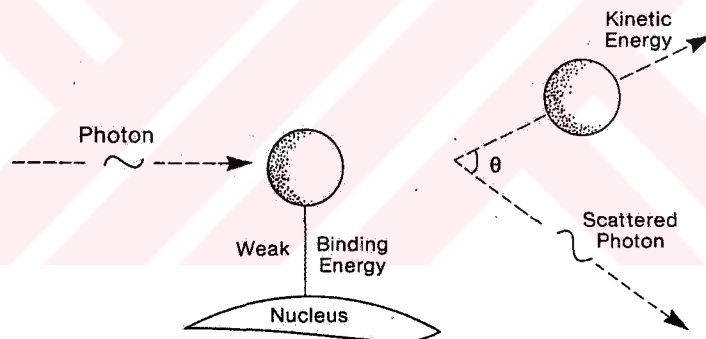
Figure 2.3 Compton Scattering [2].

2.2.3 Coherent Scattering

In coherent scattering the photon interacts with the whole atom, in contrast to incoherent scattering in which the photon interacts only with an atomic electron. The transfer of energy to the atom can be neglected due to the large rest mass of the nucleus. Coherent scattering therefore results only in a small change in the direction of the photon since the momentum change is so small.

The differential cross-section per atom is given by the classical Thompson cross-section per electron multiplied by the square of the atomic form factor *F(x,Z)*

$$\frac{d\sigma_{coh}}{d\Omega} = \frac{r_e^{\,2}}{2}\left[1 + \cos^2\theta\right]F^2(x,Z) \tag{2.6}$$

The form factor will approach the atomic number Z for interactions involving small changes in the direction of the photon and for low photon energies. The form factor decreases with increasing scattering angle. The angular distribution of coherently scattered photons is thus peaked in the forward direction.

2.2.4 Pair Production

If the energy of the incoming photon is greater than 1.022 MeV (two electron rest masses), there will be a finite probability for the photon to interact with the nucleus and to be converted into an electron-positron pair. The electron and the positron will have a certain kinetic energy and interact by inelastic collisions with the surrounding atoms. After losing its kinetic energy, the positron will annihilate with a nearby electron. To conserve energy, the annihilation creates two 511 keV photons. These are emitted in opposite directions in order to conserve momentum. The energies of the photons and the relative angle between the photons may, however, deviate slightly if the annihilation occurs in flight. The cross-section κ_{pair} is proportional to the square of the atomic number Z.

2.2.5 The Linear Attenuation Coefficient

When a photon passes through matter, any of the four interaction processes may occur. The probability for each process will be proportional to the differential cross-sections per atom (Figure 2.4 A). The probability of any interaction process to occur is given by

$$\mu = \tau_{photo} + \sigma_{incoh} + \sigma_{coh} + \kappa_{pair} \tag{2.7}$$

where μ is the linear attenuation coefficient. The mass attenuation coefficient μ/ρ is defined as the linear attenuation coefficient divided by the density ρ. The attenuation of an incoming narrow-beam of photons when passing through a non-homogeneous object can be described by

$$\Phi = \Phi_0 \exp\left[-\int_0^d \frac{\mu(\tau)}{\rho} \rho(\tau)d\tau \right] \tag{2.8}$$

where Φ is the photon fluence measured after the attenuator, Φ_0 is the photon fluence measured without the attenuator and d is the thickness of the attenuator (Figure 2.4 B).
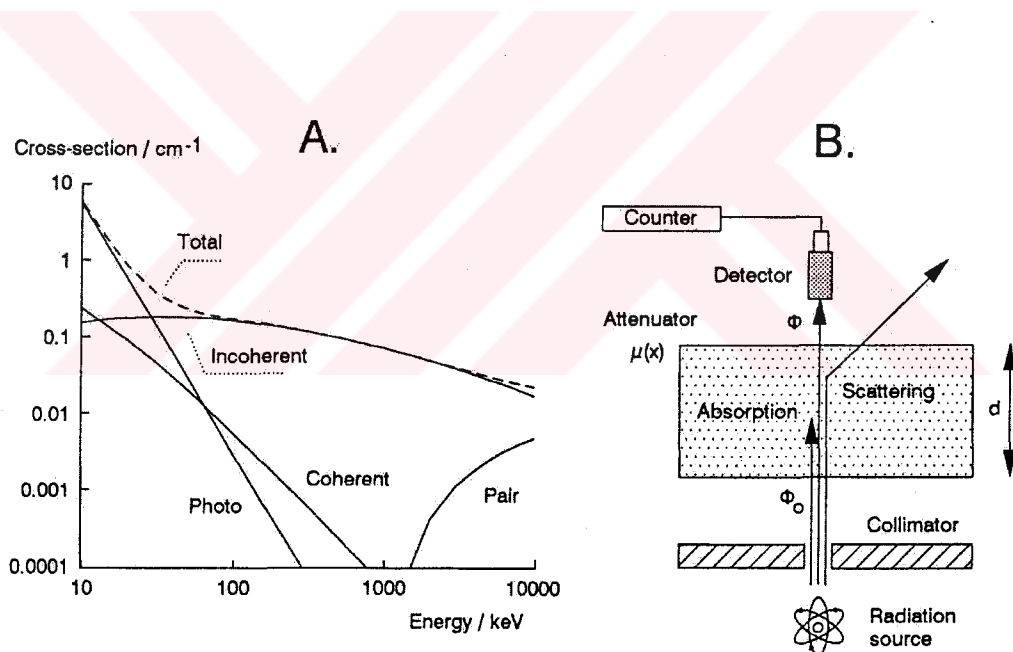
Figure 2.4 **(A)** Differential cross-sections and total attenuation coefficients for H_2O as a function of the photon energy are shown in a log-log arithmetic diagram **(B)** The conditions for narrow-beam attenuation [11].

2.3   Detector Physics

Secondary electrons are produced in photoelectric interactions, by incoherent scattering and in the pair-production. The electrons will lose their kinetic energy by subsequent inelastic collisions with other atomic electrons. The detection of ionizing radiation by measuring scintillation light, emitted as a result of the transfer of energy by secondary electrons is one of the most important techniques for radiation detection and spectroscopy. Different types of scintillator materials have been developed depending on the application. Some examples are various kinds of plastic materials, liquid scintillator solutions and inorganic compounds such as $NaI(Tl)$, $CsI(Tl)$ and $Bi_4Ge_3O_{12}$. The elements in parentheses denote certain impurities, which have been added in small amounts in order to create special sites in the lattice of the crystal, which will serve as a basis for the scintillation process.

NaI is an organic ionic crystal like other alkali halides such as NaCl, KCl and LiF. The lattices of these compounds are generally cubic and many of their properties are strongly affected by Coulomb interactions properties that have been the subject of extensive experimental and theoretical studies in the past. In addition, alkali halides are insulators whose electrons can only occupy discrete energy bands.

Liberated electrons, released from ionizing radiation, leave behind a charge deficiency that behaves like an electron with a positive charge. The size of this energy gap is approximately 8 eV and represents a broad region of the spectrum extending into the far ultraviolet where the crystal is normally transparent and photons will not be absorbed. For pure NaI, the return of an electron to the valence band with the emission of an 8 eV photon is not an efficient process and photon detection in this energy range is therefore difficult. Producing an efficient and useful scintillator with emission in the visible region of the spectrum requires the presence of localized energy states in the energy gap. Fortunately, they can be introduced by the incorporation of impurity activators into the crystal lattice. Table 2.2 lists some of the common scintillation crystals [10].

NaI(Tl) is the most frequently used inorganic scintillator. NaI(Tl) has a very high light yield, a near-linear energy response to electron and gamma rays over the energy interval 10 keV – 1000 keV, and NaI(Tl) crystals can be manufactured with quite large dimensions. The high density of NaI (3.67gcm^{-3}) and the high atomic number of iodine (Z=53) means that a large number of photo-absorption events will occur, which makes NaI(Tl) detectors suitable for spectroscopy. The instrinsic efficiency (the fraction of impinging photons detected) is about 94 percent for a 12.7-mm NaI(Tl) detector. NaI(Tl) is hygroscopic and must therefore be protected by a covering layer [11].

Table 2.2

Properties of comon inorganic scintillation crytals [10].

Material	Efficiency NaI(Tl)=100%)	Decay constant $1/e$ (ms)	Emission energy (eV)		Index of refraction	Density (g cm^{-3})	Hygroscopic
			max.	cut-off			
NaI(Tl)	100	0.23	2.99	3.87	1.85	3.67	yes
BaF$_2$	15	0.6	4	5.64	1.49	4.88	no
	2-3	0.0008	5.64	6.89			
B$_4$Ge$_3$O$_{12}$	10-12	0.3	2.58	3.54	2.15	7.13	no
CaF$_2$(Eu)	50	0.94	2.85	3.06	1.44	3.18	no
CdWO$_4$	18	5/20	2.3	2.76	2/2.4	7.9	no
CsF	3-5	0.005	3.18	4.96	1.48	4.64	yes
Cs(Na)	85	0.63	2.95	4.13	1.8	4.51	yes
CsI(Pure)	5-7	0.01	3.94	4.96	1.8	4.51	no
CsI(Tl)	45	1	2.19	3.76	1.8	4.51	no
Li(Eu)	35	1.4	2.56	2.76	1.96	4.08	yes

Bismuth germinate (B$_4$G$_3$O$_{12}$) is also one of the most frequently used scintillators. It has a stopping power higher than of NaI(Tl), which makes it suitable for use in PET systems. Like NaI(Tl), it has a cubic structure and is grown from a melt containing in this case only ultra pure GeO$_2$ and Bi$_2$O$_3$. At room temperature BGO is stable and not hygroscopic. However, BGO is relatively expensive and is not available in very large sizes.

The dead time restricts the possibility for any detector to measure high count rates. This is determined by the time required to process an event and the ability to process events simultaneously. The energy pulse from a scintillation detector can be characterized by a very fast rise time and an exponential decay time.

The scintillation light is detected in an amplifying photo-multiplier tube (PMT), which basically consists of a photocathode, and several dynodes sealed in a vacuum tube. Each dynode is coated with a special material, which responds to an incoming photoelectron by emitting two or more secondary electrons. When an incoming photon strikes the photo-cathode, photo-electrons are emitted. The photo-electrons are rapidly accelerated towards the next dynodes and knock out a further two or more new electron. The result is an avalanche of electrons, which is collected by an anode at the end of dynode chain. Figure 2.5 shows the structure of an eight-stage, box-and-grid, head-on PMT with a 60mm hexagonal window. It employs a potassium-caesium-antimonide (bialkali) photo cathode and has a gain of 1.9×10^5 at 800 V.
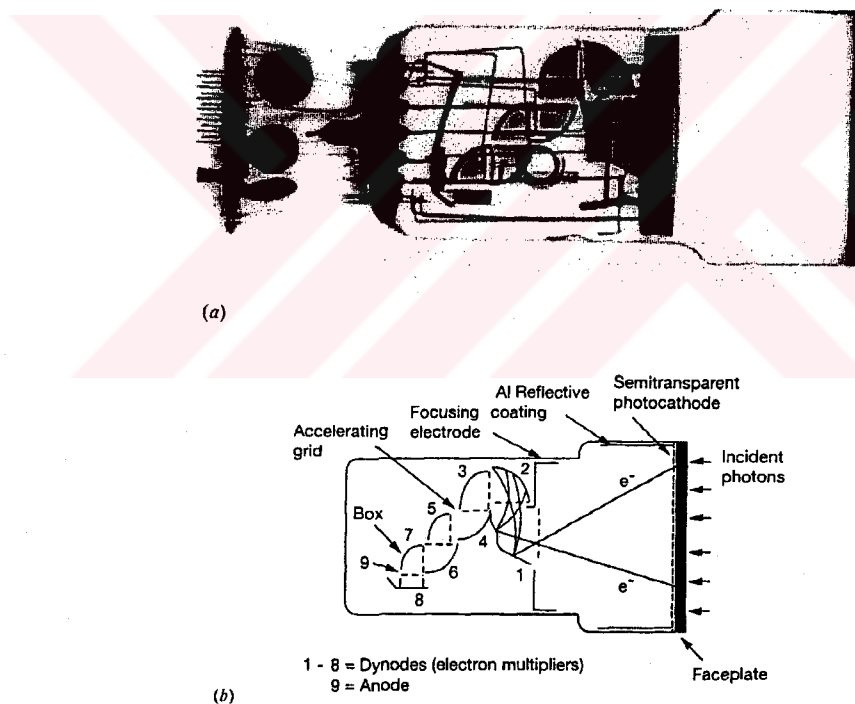
Figure 2.5 A PMT (a) Structure of PMT (b) Schematic diagram.

The conversion of scintillation light to detectable energy signals is not a linear process. It involves statistical fluctuations, mainly in the detection for the scintillation photons, but also from electronic noise and variation in the detection response over the photo-cathode surface. These fluctuations result in a broadening of the detected scintillation pulses and this in turn means that the energy pulse-height distribution

measured has a Gaussian shape. The performance of any detector when detecting photons of different energies may therefore be characterized by the energy resolution, $R = \Delta E/E$, where ΔE is the full width at half maximum (FWHM) of the photo-absorption peak in the energy pulse height. Distribution and E is the photon energy corresponding to the peak value. The FWHM is proportional to the square root of the energy imparted [10].

3. Gamma Camera

Nuclear medical imaging, also called nuclear medicine, is based on detecting nuclear radiation emitted from the body after introducing a pharmaceutical inside the body to tag a specific biochemical function. A schematic illustration of a gamma camera is given in Figure 3.1.
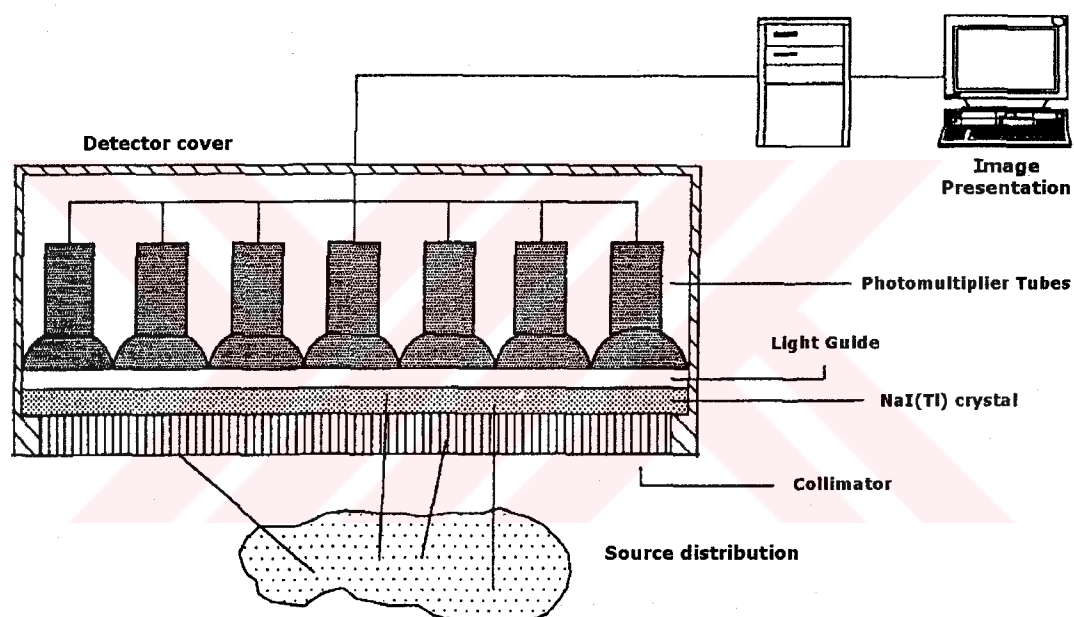
Figure 3.1 A schematic illustration of gamma camera [11].

The scintillation camera was invented by Hal O Anger in 1956. In 1962, the first commercial camera was presented by Nuclear Chicago, with a NaI(Tl) crystal 25 cm in diameter and thickness 1.25cm, with 19 photomultiplier tubes (PMT). With the development of techniques for growing larger NaI(Tl) crystals, cameras with wider fields view developed from the mid-1970s. Although ^{99m}Tc was discovered as early as 1938, it was not until the middle of the 1960s that ^{99m}Tc-labelled radiopharmaceuticals became widely available. ^{99m}Tc decays emitting optimal photon energy of 140.5 keV for scintillation camera imaging and has favorable dosimetric properties [10].

The scintillation camera is the most commonly uses imaging system in nuclear medicine today for both planar and tomographic studies. The photon energy range is covered from 40-50 keV up to 400 keV normally. Some cameras are shielded and are useful up to 511keV, so with these cameras positron-emitting radionuclides/pharmaceuticals can be studied. Gamma camera system is composed of scintillation camera head(s), gantry, and computer. The computer is generally separated into acquisition and processing stations. The components together make up an integrated system.
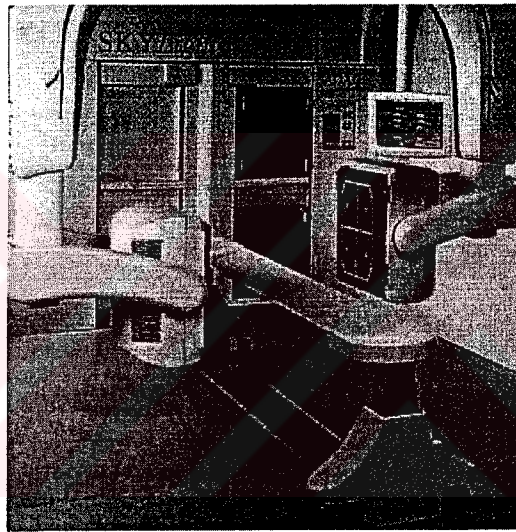
Figure 3.2 A modern two-headed gamma camera.

3.1   Principles

A gamma camera, also called the scintillation camera, converts photons emitted by the radionuclide in the patient into a light pulse and subsequently into a voltage signal. This signal is used to form an image of the distribution of the radionuclide [8].

Photons emitted from the activity distribution in the patient are projected through the collimator onto the sodium iodine crystal, where they interact and create scintillation light. The light is detected by photomultiplier tubes (PMTs), and transformed into current

pulses, proportional to the flux of the incoming photons. These pulses are processed by analogue and/or digital electronic circuits, and computation with suitable algorithms results in output signals (data) representing the scintillation light distribution created in the crystal, and the energy deposited in the crystal.

3.2   Components of a Gamma Camera

The basic components of a gamma camera imaging system are the collimator, the scintillation crystal (detector), an array of photomultiplier tubes, a pulse height analyzer (PHA), and a cathode ray tube for displaying images.

3.2.1   Collimator

A collimator is the first processing layer of a gamma camera to encounter photons from radioactive source. If the detector were exposed to radiation without some sort of shielding there would be no way of knowing from which direction the radiation came. A collimator is essentially a block of lead larger than the detector, containing an arrangement of holes, which allows gamma rays to pass through from a specified direction. The lead thickness is sufficient to absorb unwanted radiation.

There are broadly four types of collimators: parallel hole, converging, diverging, and pinhole [8]. The standard collimator mostly in use with the scintillation camera is the parallel-hole collimator. There are also slanthole and fan-beam collimator types.

Parallel-Hole: A common arrangement is for the collimator holes to be parallel, as illustrated in Figure 3.3. The field of view (FOV) is determined by the size (diameter) of the crystal and remains the same at all source-to-camera distances.
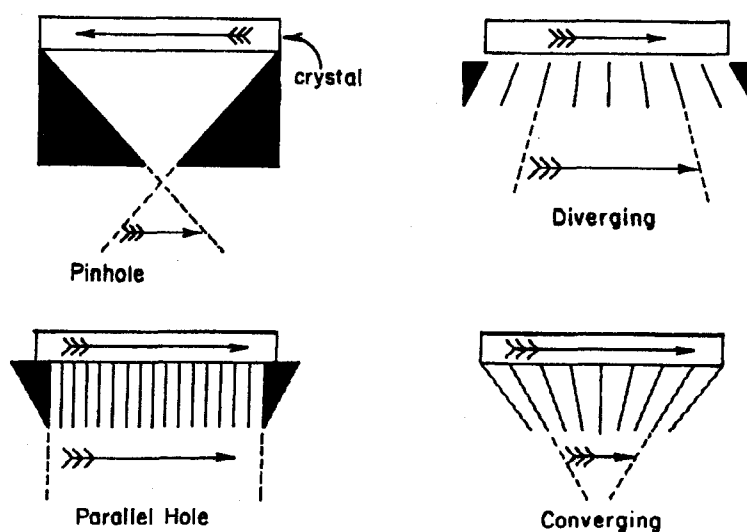
Figure 3.3 Types of gamma camera collimators [8].

Diverging collimators: In the diverging collimator, the holes fan out from the surface of the crystal, as shown in Figure 3.3. With this arrangement of holes, the camera can image a source larger than the crystal. Generally, use of a diverging collimator increases the imaged area by about 30% over that obtained with a parallel-hole collimator. The image itself, however, is slightly minified. Diverging collimators are used particularly on cameras with small crystal faces to image large organs, such as the lungs.

Converging Collimators: The holes in the converging collimator are arranged so that they point to, or converge on, a point located in front of the collimator. This is the reverse arrangement of the diverging collimator. In fact, some collimators are reversible so that they can be used as either a diverging or converging collimator. The converging collimator produces image magnification. The degree of magnification depends on the design of the collimator and the distance from the collimator surface. Because of its magnification properties, the converging collimator is useful for imaging small organs, such as the thyroid gland, kidneys, and heart.

Pin-Hole Collimator: The pin-hole collimator differs from other collimators in that it has a single small hole rather than several thousand holes (Figure 3.3). The basic principle of this collimator is the same as that of the pin-hole camera from the early days of photography. The "lens" of the camera is a small hole (pin-hole) in an absorbing material. Radiation from each point within the body is limited to a corresponding point on the

crystal as the radiation passes through the hole. This creates an image of the source on the crystal surface. With a pin-hole collimator, the orientation of the image at the crystal surface is inverted.

Slanthole collimator: A variation of the Parallel hole is the Slanthole collimator (Figure 3.4), which has all tunnels slanted at a specific angle. It generates an oblique view for better visualization of an organ, whose view is partly or totally blocked by other parts of the body. As an advantage, this collimator can be positioned close to the body for the maximum gain in resolution.
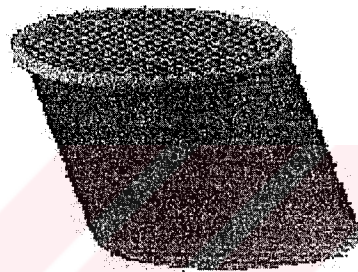
Figure 3.4 Slant hole collimator [14].

Fan-beam collimators: The Fan-beam collimators (Figure 3.4) are designed for a rectangular camera head to image smaller organs like the brain and heart. When viewed from one direction, the holes are parallel. When viewed from the other direction, the holes converge. This arrangement allows the data from the patient to use the maximum surface of the crystal.
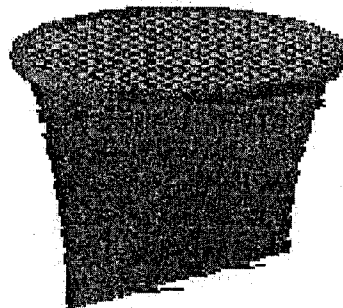
Figure 3.5 Fan-beam collimator [14].

Typically, a gamma camera is equipped with several interchangeable collimators. The differences among the collimators are the thickness, number- and size of the holes and the way they are arranged or oriented.

3.2.2 Crystal

To absorb the gamma photons and to convert the gamma image into a light image is basic function of the crystal in the gamma camera. Radiation emitting from the patient and passing through the collimator may interact with a thallium-activated sodium iodide crystal. Interaction of the gamma ray with the crystal may result in ejection of an orbital electron (photoelectric absorption), producing a pulse of fluorescent light (scintillation event) proportional intensity to the energy of the gamma ray. PMTs situated along the posterior crystal face detect this light and amplify it. The crystal is fragile and must have an aluminum housing that protects it from moisture, extraneous light, and minor physical damage.

3.2.3 Photomultiplier Tube (PMT)

A PMT converts a light pulse into an electrical signal of measurable magnitude. An array of these tubes is situated behind the sodium iodide crystal and may be placed directly on the crystal, connected to the crystal by light pipes, or optically coupled to the crystal with a silicone-like material. In addition to converting the light from the crystal into electrical pulses and amplifying the pulses, the PMT array also detects where each gamma photon is absorbed in the crystal.

A scintillation event occurring in the crystal is recorded by one or more PMTs. Localization of the event in the final image depends on the amount of light sensed by each PMT and thus on the pattern of PMT voltage output. The summation signal for each scintillation event is then formed by weighing the output of each tube. This signal has three

components spatial coordinates on X and Y-axes as well as a signal (Z) related to intensity. The X and Y coordinates may go directly to instrumentation for display on the CRT or may be recorded in the computer. The signal intensity is then processed by the PHA.

3.2.4   Pulse Height Analyzer (PHA)

The basic principle of the PHA is to discard signals from background and scattered radiation or radiation from interfering isotopes, so that only photons known to come from the photopeak of the isotope being imaged are recorded. The PHA discriminates between events occurring in the crystal that will be displayed or stored in the computer and events that will be rejected. The PHA can make this discrimination because the energy deposited by a scintillation event in the crystal bears a linear relation to the voltage signal emerging from the PMTs.

Signal intensity information is matched in the PHA against an appropriate window, which is really a voltage discriminator. To allow energy related to the desired isotope photopeak to be recorded, the window has upper and lower voltage limits that define the window width. Thus, a 20% symmetric window for 140-keV photopeak means that the electronics will accept 140 ± 14 keV- (i.e., 140 keV $\pm$ 10%) gamma rays. Any signals higher or lower than this, particularly those from scattered radiation, are rejected.

3.2.5 Cathode Ray Tube (CRT)

Most conventional viewing units create the image on the screen of a cathode ray tube (CRT), more commonly known as a picture tube.

3.3   IMAGE FORMATION

Photons emitted from the patient are mechanically collimated by an appropriate collimator. The collimated radiation is incident on the NaI(Tl) crystal at "point" (x, y) giving rise to visible light or scintillation in a small region surrounding *(x, y)*. The scintillation light is guided toward the photocathodes of the photomultiplier tubes optically coupled to the NaI(Tl) crystal. Since light spreads while traversing the thickness of the crystal, the photocathodes view a small disc of light, quantified in terms of a light spread function. The scintillation light is divided among the bank of photomultiplier tubes in proportion to its proximity to each tube [2].

Each tube converts the light it receives to a voltage pulse at its anode. Thus the height of the output pulse from each tube is proportional to the total light received by each tube's photocathode. The patterns of voltage pulses from each tube are fed to analog or digital positioning circuitry to determine uniquely the location, that is, the x and y coordinates of each scintillation event on the crystal. The output from each tube is summed to produce a net signal proportional to the total energy deposited in the crystal by the scintillating event. This signal is referred to as the "z signal." Pulse height discrimination is applied to the z signal to retain only those events where the total energy deposited in the crystal lies within a prescribed energy window. The *(x, y)* coordinates of each count passing the pulse height discrimination are stored to a projection image where the projection axis is normal to the plane of the collimator. Then the obtained image is shown on the viewing unit.

4. CAMERA CHARACTERISTICS AND IMAGE QUALITY

This chapter focuses on gamma camera characteristics and how these characteristics depend on its various components.

4.1 Sensitivity

In a typical imaging situation, only a small fraction of the gamma photons emitted by the radioactive material contribute to the formation of the image. The only photons that contribute to the image are the ones passing through the appropriate collimator hole and absorbed in the crystal. Photons from the source that are not absorbed in the crystal wasted and do not contribute to image formation. This characteristic of a gamma camera is generally referred to as sensitivity. The sensitivity of a camera can be described in terms of number of photons detected and used in the image for each unit (μCi) of radioactivity.
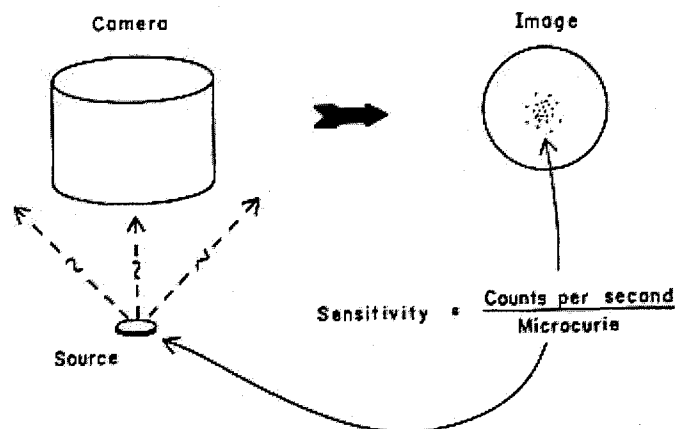
Figure 4.1 The concept of gamma camera sensitivity [2].

The thickness of a scintillation crystal has an effect on detector efficiency. Detector efficiency and camera sensitivity are reduced when photons pass through the crystal. Therefore, a thick crystal tends to yield higher sensitivity, especially for high-energy photons, but also produces more image blur.

Another factor that affects the sensitivity of a camera system is the setting of PHA. The only photons that contribute to the image are the ones within the PHA window. A window that is very small or incorrectly positioned with respect to the photon energy spectrum can significantly reduce camera sensitivity.

Many cameras have a short dead time after each photon is detected during which an arriving photon is not counted. Dead time reduces sensitivity when the photon rate is high and the photons tend to overlap.

Camera sensitivities are generally in the range of 100 to 1000 cps/μCi. Since 1 μCi typically yields 37000 photons per second, this means less than 3% of the emitted photons are used for image formation [2].

4.2   Collimator Characteristics

The performance of a collimator is measured by three quantities: Resolution, efficiency, and septum penetration, which are determined by the three collimator dimensions height, hole diameter, and septum thickness. The only additional variable is the hole shape such as round, hexagonal, square, triangular, and straight or tapered.

Resolution is the quantity most directly related to the amount of detail visible in the image. Sensitivity is the measure of the counting efficiency of a system and includes the detector efficiency as well as the collimator geometric efficiency. Further, the efficiency is defined for a collimator depends on whether the source distribution it is viewing is a point source, line source, area source, or volume source. Collimator sensitivity refers to the percentage of incident photons that pass through the collimator [9]. A collimator that yields maximum sensitivity usually produces maximum image blur.

The lead walls between the holes are referred to as septa. The purpose of the collimator septa is to prevent photons from penetrating from one hole to another. When selecting a collimator, it is necessary to consider the energy of the gamma photons. The ability of a photon to penetrate a given material generally increases with photon energy. Therefore, it takes a thicker piece of material to absorb high-energy photons than it does to absorb low-energy photons. Therefore, a collimator for high-energy gamma rays has much thicker septa than a collimator for low-energy rays. The septa are generally designed so that septal penetration by unwanted gamma rays does not exceed 10% to 25%. With low-energy photons, relatively thin septa are adequate. The advantage of thin septa is that more holes can be located in a given area, and this results in a higher sensitivity. However, thicker septa must be used with high-energy photons in order to prevent photons from crossing over from one hole to another.
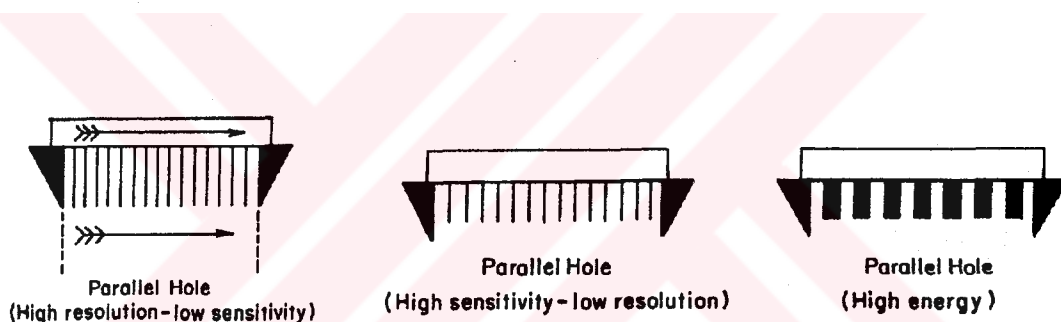
Figure 4.2 Parallel hole collimators. Energy, resolution, sensitivity [8].

Comparison of low-energy and high-energy collimators is shown in Figure 4.3. If a low-energy collimator is used with high-energy photons, significant septal penetration will occur, and the image will be abnormally blurred. If a high-energy collimator is used with low-energy photons, an image of normal quality will be obtained, but the camera will be operating with less than optimum sensitivity.
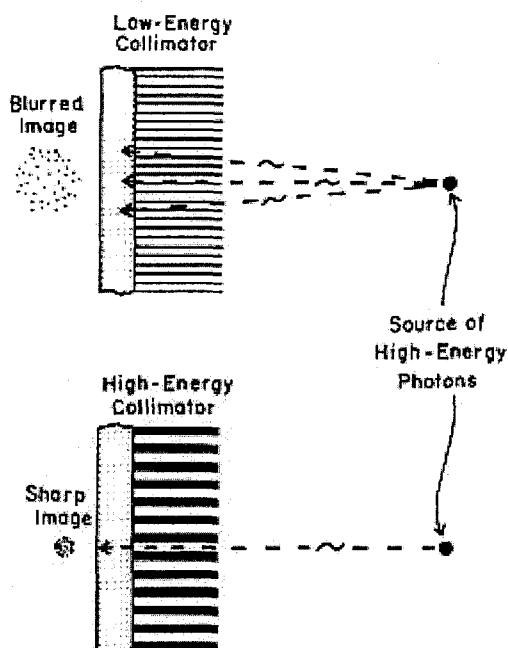
Figure 4.3. Comparison of low-energy and high-energy collimators [2].

An appropriate collimator should be chosen to correspond to the energy of the isotope being imaged. Low-energy collimators generally refer to a maximum energy of 150 keV, whereas medium-energy collimators have a maximum suggested energy of about 400 keV Collimators are available with different lengths and different widths of septa. In general, the longer the septa, the better the resolution but the lower the count rate (sensitivity) for a given amount of radionuclide. The count rate is inversely proportional to the square of the collimator hole length. If the length of the septa is decreased, the detected count rate increases, and resolution decreases (Figure 4.4).
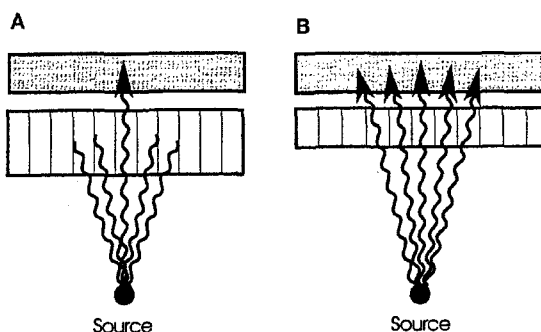
Figure 4.4 Effect of septal length on collimator sensitivity and resolution. (A) Longer septa. (B) Shorter septa [8].

As shown in Figure 4.4 longer septa in the collimator attenuate most photons, except those exactly perpendicular to the crystal face. This increase in selectivity increases the resolution and decreases the count rate detected. Shortening the length of the septa allows more photons to reach the crystal; thus, the count rate is higher. The spatial resolution is decreased because the photons coming through a hole in the collimator are from a larger area.

The difference between typical low-energy, general-purpose collimators and low-energy, high-sensitivity collimators is that high-sensitivity collimators may allow about twice as many counts to be imaged, although the spatial resolution is usually degraded about 50%. Thus, a high-resolution, low-energy collimator has about three times the resolving ability of a high-sensitivity, low-energy collimator. Most collimators are now designed with hexagonal rather than round holes. Because they have overall thinner septa, they have greater sensitivity but more septal penetration than collimators with square or round holes.

With a parallel-hole collimator, neither the size of the image nor the count rate changes significantly with the distance of the object of interest from the collimator. This is because as the object is moved small distances away from the crystal, the inverse square law reduces the number of counts. However, this is compensated for by the increased viewing area of the collimator. On the other hand, resolution is best when the object of interest is as close to the collimator face as possible, and scans with multihole collimators are usually obtained with the collimator in contact with or as close as possible to the patient.
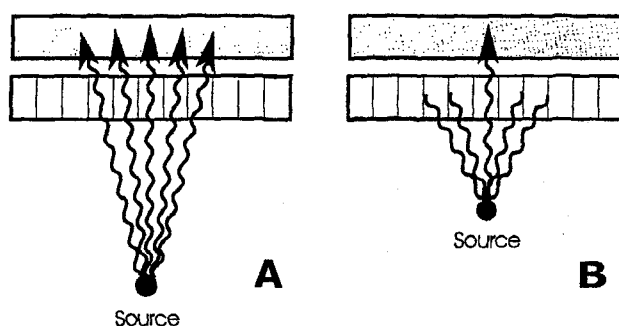
Figure 4.5 Effect of different source-to-camera distances [8].

With the source a long distance from the camera head, a large number of photons can reach the crystal in an almost perpendicular fashion. The large area of impact on the crystal increases uncertainty about the exact location of the source. As the source is brought closer to the camera head, the correspondence of the scintillation event in the crystal with the actual location is much better, and resolution is improved. (Figure 4.5)
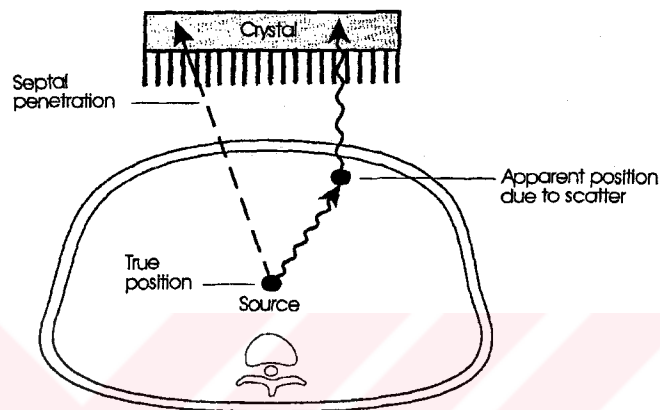
Figure 4.6 Scintillation events that degrade images [8].

With a parallel-hole collimator, scattered photons emitted from the patient perpendicular to the crystal face may be imaged (Figure 4.6). These photons and those that penetrate the septa cause degradation of spatial resolution. Both septal penetration and photon scattering within the patient's body cause events to be recorded in locations other than their true positions.

4.3 FIELD OF VIEW (FOV)

The field of view (FOV) of a gamma camera is an important characteristic because it determines how much a patient's body can be imaged at any one time. The FOV depends on the size of the crystal, the type of collimator, and, in some systems, the distance between the object being imaged and the camera crystal. In the following part the differences of FOV of various types of collimators, and their effect on sensitivity is discussed.
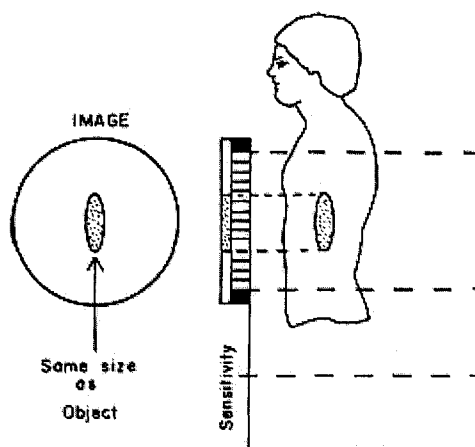
Figure 4.7 Parallel-hole Collimator [2].

With parallel-hole collimators the FOV is determined by the size of the crystal and it is independent of source-to-camera distances. Therefore, the parallel-hole collimator does not produce either magnification or minification of the image. Assuming there is no photon absorption between the source and collimator, the number of the photons does not change significantly with the source-to-camera-distance. So, camera sensitivity with a parallel-hole collimator is generally not affected by changing the distance between the source and camera.

In the diverging collimator, FOV increases with distance from the face of the collimator. The major advantage of the diverging collimator is the increased FOV. The rate which the FOV increases with distance depends on the angulation of the holes. The increase in the FOV causes minification of the object imaged. The degree of minification increases with the distance between the source and collimator. The change in minification increases with distance can produce distortion in the image, because objects close to the camera are minified less than objects located at a greater distance from the camera surface.

The sensitivity of a camera quipped with a diverging collimator decreases with distance between the source and camera. As the radioactive source is moved away from the collimator, it is in the FOV of a smaller number of holes. This reduces the number of photons that reach the crystal and decreases camera sensitivity.
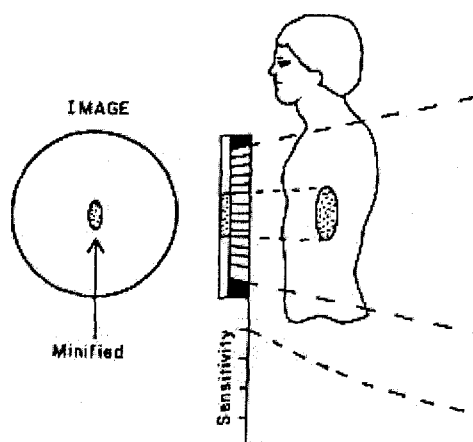
Figure 4.8 Diverging Collimator [2].

The FOV for a converging collimator decreases with increased distance between the source and collimator. Therefore, converging collimators produce image magnification. As a radioactive source is moved away from the collimator, it comes into the view of more collimator holes, and this produces an increase in the sensitivity until it reaches the focal point, beyond which sensitivity begins to decrease. The sensitivity increases approximately as the square of the distance from the collimator. However, resolution decreases with distance, and converging collimators produce distortion around the edges.
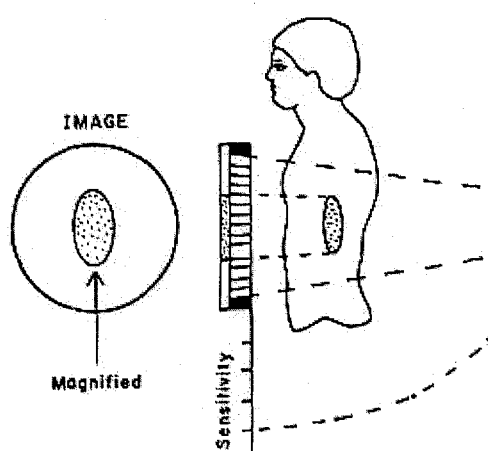
Figure 4.9 Converging Collimator [2].

The FOV of a pin-hole collimator is very dependent on the distance between the source and the collimator. When the source is located as far in front of the collimator as the crystal is behind the collimator, the FOV is equal to the size of the crystal. If the source is located closer, the image will be magnified. The degree of magnification increases as the source approaches the collimator. Because it has only one hole, the sensitivity of the pin-hole collimator is obviously less than for typical multihole collimators. It also decreases as the distance between the source and pin-hole is increased. In many cameras, the pin-hole can be changed. A large hole gives more sensitivity, but also more blur.
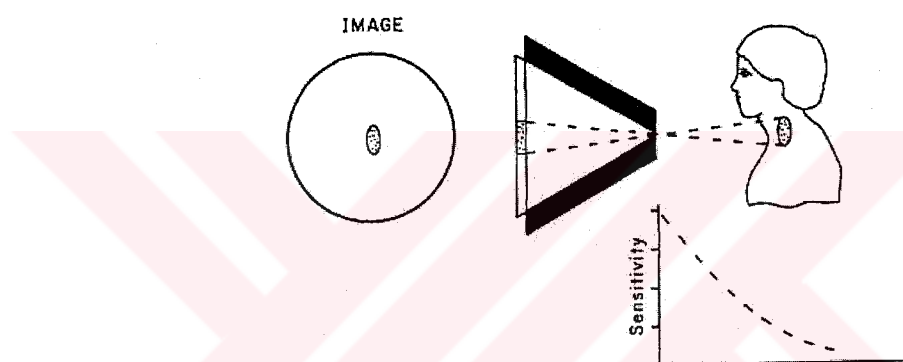
Figure 4.10 Pin-hole collimator [2].

4.4 Crystal Characteristics

Both dimensions, diameter and thickness of the crystal, have an effect on the characteristics of the camera. The diameter of the crystal establishes the basic FOV, which is then modified by the type of collimator used and the distance between the camera and he source being imaged. The thickness of the crystal affects sensitivity and image blur. Increasing crystal thickness generally decreases crystal penetration and improves sensitivity. However increasing the thickness also increases image blur. Therefore, crystal thickness provides a reasonable compromise between sensitivity and image blur.

The crystal may be 25 to 66 cm in diameter and 0.635 to 1.5 cm thick. For most cameras, a 0.935-cm-thick crystal is used. A larger-diameter crystal has a larger field of view and is more expensive but has the same inherent resolution as a smaller-diameter crystal. The thicker the crystal becomes, the worse the spatial resolution but the more efficient the detection of gamma rays. In general, with a 1.25-cm-thick crystal, the efficiency for detection of gamma rays from xenon 133 (^{133}Xe) (81 keV) and technetium 99m (^{99m}Tc) (140 keV) is almost 100%; that is, few of the photons pass through the crystal without causing a light pulse. As the gamma energy of the isotope is increased, the efficiency of the crystal is markedly reduced. For example, with iodine 131 (^{131}I) (364 keV), efficiency is reduced to about 20% to 30%. With a thinner crystal, the overall sensitivity (count rate) decreases by about 10% because more photons pass through, but there is about a 30% increase in spatial resolution because the PMTS are closer to the event and thus can localize it more accurately, and because there is an increase in light collection.

4.5   PMT Characteristics

The light interaction caused by a gamma ray generally occurs near the collimator face of the crystal. Thus, although a thicker crystal is theoretically more efficient, the PMT is farther away from the scintillation point with a thick crystal and is unable to determine the coordinates as accurately. Therefore, spatial resolution is degraded. The number of PMTS is also important for the accurate localization of scintillation events; thus, for spatial resolution, the greater the number of PMTs, the greater the resolution. The early gamma cameras used 19 round PMTS, whereas newer cameras use up to 115 hexagonal, square, or round PMTS with diameters 1.5-7.5 cm.

4.6   PHA Characteristics

In many nuclear medicine procedures, it is desirable for the counting or imaging system to respond only to radiation from a specific primary source within the patient or sample. A problem arises because radiation from other sources might be present and enter the detector. Also, some of the radiation from the primary source undergoes Compton interactions with materials outside the source volume. This produces scattered radiation, which can enter the detector. If an imaging system responds to this scattered radiation, the resulting image will include areas around the primary source. This distorts the image and makes it impossible to determine the actual size, shape, and activity of the primary source organ or lesion. Radiation from other sources might also be present. Cosmic radiation, naturally occurring radioactive nuclides in building materials, and radioactive contamination of the environment produce what is generally referred to as background radiation. Background radiation can reduce contrast in images and introduce errors into the counting of radioactive samples. Occasionally, two radioactive materials are administered to a patient, and the system must selectively respond to each source at the appropriate time.
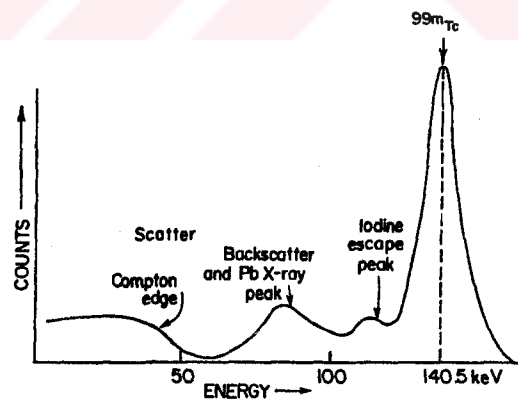
Figure 4.11 Energy spectra for technetium 99m when viewed by the gamma camera as a point source [8].

A typical energy spectrum from a PHA is shown in Figure 4.11. The photopeak is the result of total absorption of the major gamma ray from the radionuclide. If the characteristic K-shell x-ray of iodine (28 keV) escapes from the crystal after the gamma ray has undergone photoelectric absorption, the measured gamma ray energy for 99mTc would be only 112 keV (140 minus 28 keV). In other words, the detector sees only 112

keV rather than 140 keV. This gives rise to a spectrum component generally referred to as an iodine escape peak. The energy of an iodine escape peak is always 28 keV below photopeak energy.

A backscatter peak may result from primary gamma rays' undergoing 180-degree scatter and then entering the detector and being totally absorbed. This can occur when gamma rays strike material behind the source and scatter back into the detector. It may also occur when gamma rays pass through the crystal without interaction and Compton scatter from the shield or PMTS back into the crystal.

The lead x-ray peak is due to primary gamma rays undergoing photoelectric absorption in the lead of shielding or the collimator; as a result, characteristic x-rays (75 to 90 keV) are detected.

Compton Scatter: When a gamma photon is engaged in a Compton interaction with a material, it both loses energy at the site of interaction and changes direction. Compton interactions can take place between the photon and the material containing the radioactive source, the detector crystal, or material located between the source and crystal. In radionuclide imaging procedures, a significant number of Compton interactions usually occur in the tissue surrounding the radioactive material. If these scattered photons are included in the image, the image will not be a true representation of the distribution of radioactive material.
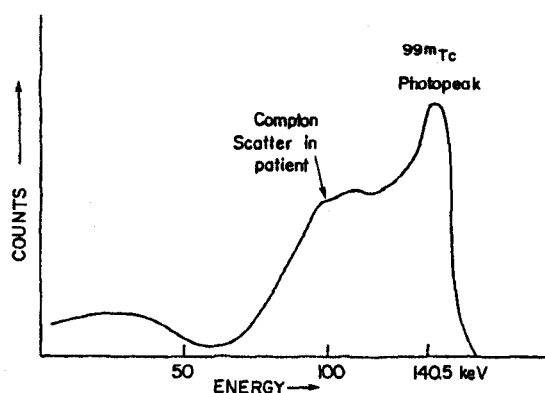
Figure 4.12 Energy spectra for technetium 99m when viewed by the gamma camera as a point source in a patient.

For a given primary energy, such as 140 keV, the energy of the scattered photon depends on the angle of scatter. Scatter that takes place within the body adds a component to the spectrum, as shown in Figure 4.12. Photons that scatter in the forward direction (directly toward the detector) lose very little energy in the scattering interaction and have energies very close to 140 keV. The statistical fluctuation within the detector causes some of these to appear to have energies greater than 140 keV. The fluctuations within the detector system cause the overlap between the scatter component and the photopeak of the spectrum. Photons that scatter in the backward direction (180°) have the lowest energy. For 140-keV primary photons, complete backscatter produces 90-keV photons. This means that the scattered radiation produced by a 140-keV primary source has photon energies ranging from 90 keV to 140 keV. However, some photons may undergo two or more Compton interactions before leaving the body, and this creates some photons with energies well below 90 keV. The exact shape of the scatter portion of the spectrum and its amplitude relative to the photopeak depend on a number of factors, especially the thickness of tissue covering the radioactive material.

If Compton interactions take place within the detector crystal, a different spectrum component is created. The spectrum represents energy deposited within the detector. If a 140-keV photon undergoes a single Compton interaction in the crystal, the maximum energy it can deposit is 50 keV. This occurs when the photon is scattered back out of the crystal (180°) and carries an energy of 90 keV. The energy deposited in the crystal (50 keV) is the difference between the primary photon energy (140 keV) and the scattered photon energy (90 keV). Photons that scatter in a more forward direction have higher energies and therefore deposit less energy in the crystal. The effect of Compton scattering in the detector gives a peak from 0 to 50 keV. The high-energy side of this spectrum component is known as the Compton edge.
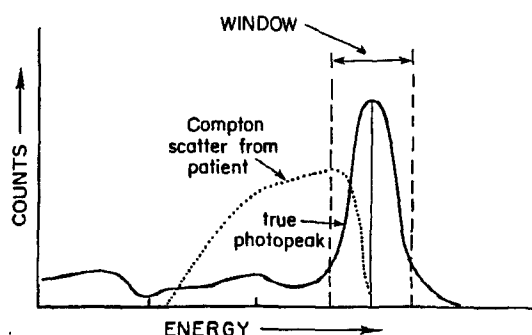
Figure 4.13 PHA window positioning [8].

PHA settings should be considered in relation to the photon energy spectrum, as illustrated in Figure 4.13. The window settings determine the portion of the spectrum that will be used for imaging or data collection. The window is generally positioned over the desired portion of the spectrum, such as the photopeak. The area under the spectrum curve that falls within the window represents the relative number of photons that are being collected and used. A wide window setting, which encompasses more of the spectrum, produces an increase in the rate at which photons are counted. With a wide window, an image can be formed faster, or a certain number of counts can be collected in a shorter period. The problem with increasing window width is that it decreases the ability to discriminate between the desirable and undesirable portion of the spectrum.

4.7   Resolution

Resolution is one of the common performance parameters for gamma cameras. Typical performance characteristics of state-of-the art cameras are shown in Table 4.1. Resolution usually refers to either spatial or energy resolution. Spatial resolution refers to the ability to display discrete but contiguous sources of radioactivity. The spatial resolution of various gamma camera systems is usually given in terms of either inherent or overall resolution. Instrinsic Resolution (Inherent spatial resolution) *is* the ability of the crystal PMT detector and accompanying electronics to record the exact location of the light pulse

on the sodium iodide crystal. Marked improvements in gamma cameras have allowed an instrinsic resolution of about 3 mm.

Table 4.1
Typical gamma Camera performance characteristics.

Spatial (Instrinsic) resolution (FWHM)	3-5 mm
Energy resolution	10%-14%
Temporal resolution	100-350k counts/s
Field uniformity	2% to 5%

Statistical variability is particularly important in resolution. An event occurring exactly between two PMTs does not always give the same number of photons to each tube; thus, for any single event, the distribution of photons is statistically variable. Statistical variation is relatively greater when fewer light photons are available. In other words, the instrinsic resolution of a system or its ability to localize an event is directly related to the energy of the isotope being imaged. When radioisotopes with low-energy gamma rays are used, the camera has less inherent spatial resolution.

Another factor that affects inherent (instrinsic) resolution to a minor extent is Compton scatter. When the gamma ray interacts with the crystal, there is usually photoelectric absorption, which results in a light pulse at the point of interaction. With higher-energy gamma rays, however, the initial event may be a Compton interaction or scatter (i.e., a collision between a gamma ray and a loosely bound orbital electron). This results in scattered photons with light coming from several points, even though only a single gamma ray interacted with the crystal initially.

Overall spatial resolution is the resolution capacity of the entire camera system, including such factors as the collimator resolution, septal penetration, and scattered radiation. When the overall spatial resolution of the system with high-energy isotopes is considered, the limiting resolution is that of the collimator. When low-energy isotopes are imaged, the intrinsic resolution becomes more important than the collimator resolution. As

the energy of the incident gamma ray decreases, the intrinsic resolution of the crystal decreases markedly because the lower-energy Gamma rays provide less light for the PMTs to record; thus, there is more statistical uncertainty regarding the origin of the gamma ray. Although the intrinsic resolution is very important, the overall resolution determines the quality of the image because it is a combination of the resolutions of each of the components in the imaging chain, including the Collimator, the inherent resolution, septal penetration, and scatter. The overall system resolution (R_s) is

$$R_s = \sqrt{R_i^2 + R_c^2} \tag{4.1}$$

where R_i^2 is inherent spatial (instrinsic) resolution and R_c^2 is collimator resolution.

Another category of resolution is energy resolution. The variation in pulse size causes the pulse spectrum to assume the form of a broadened peak rather than a narrow line. Amount of variation in pulse size, or spreading, of the spectrum it produces is known as energy resolution. Energy resolution generally expressed in terms of the full width at half maximum (FWHM). The FWHM is the full width of the spectrum peak measured at one-half of the maximum height of the peak. It is generally expressed as a percentage of the average pulse size (photon energy). It is shown in Figure 4.14.
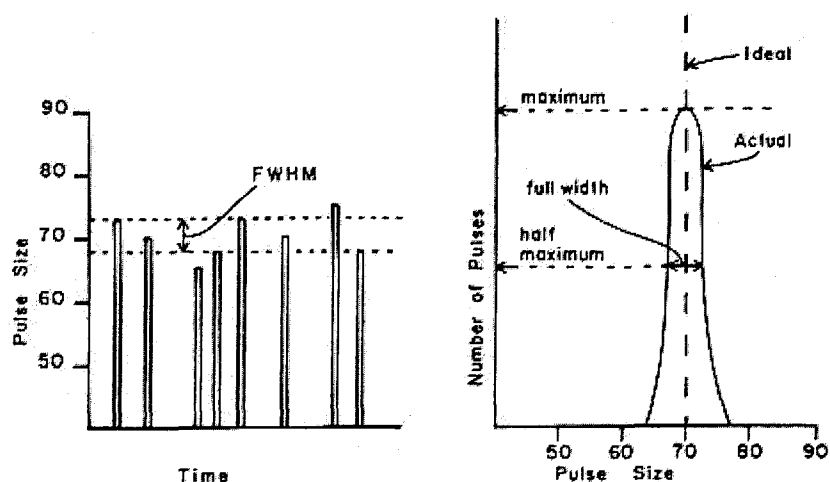
Figure 4.14 Pulse spectrum produced by a monoenergetic radiation source and The full width at half maximum [2].

The FWHM might be considered as an expression of the average variation in pulse size. The ideal detector system would have an FWHM of 0. Actual scintillation detector systems generally have an energy resolution capability (FWHM) of approximately 10% to 14%. This resolution values allow use of 15% to 20% energy windows to encompass all the photons of interest. The energy resolution of a detector system generally depends on the overall quality of the crystal and PM tube and the stability of the pulse amplifier. Severe loss of energy resolution capability can result from conditions such as a fractured crystal or inadequate light transmission between the crystal and PM tube.

Poor energy resolution, or high FWHM values, means that the pulse size associated with the monoenergetic photons from the primary source varies considerably. This makes it difficult for the PHA to separate these pulses from the pulses arising from other radiation sources.

4.8 Count Rate and Dead Time

As with any detection system, it is important that scintillation events do not occur so fast that the electronic system is unable to count each as a separate event. If two equal light pulses occur too close together in time, the system may perceive this as one event with twice the energy actually present. Such an occurrence of primary photons would be eliminated by the energy window of the PHA, and none of the information from the two events would be imaged; thus, the sensitivity of the system would be diminished. A more significant problem is loss of spatial resolution when several scattered (low-energy) photons strike the crystal at the same time, so that their light production is summed and appears as a photon of interest. The time after an event during which the system is unable to respond to another event is referred to as dead time. Dead time can be important in high-count-rate dynamic studies (in the range of 50,000 counts/s), particularly with single-crystal cameras.

4.9   Field Uniformity

Despite the efforts of manufacturers to produce high-quality collimators, crystals, PMTs, and electronics, nonuniformity inevitably occurs. One direct effect is variation in the pulse-height distribution, where the full energy peak will shift between different channels. Acceptable field nonuniformity is on the order of 2% to 5%. Much of this can be corrected by the computer system.

4.10   Intrinsic Linearity

Intrinsic linearity is the ability of the detector (without collimator) to image radioactive line sources as straight lines in the image. Two types of measure are given, intrinsic spatial differential and absolute linearity: (a)differential linearity is the standard deviation of the deviation from that line in the image and; (b)the absolute linearity is the maximum displacement. Typical values of differential linearity for modern cameras are of the order of 0.2-0.5 mm.

5. MONTE CARLO METHOD

Monte Carlo numerical simulation methods can be described as statistical methods that use random numbers as a base to perform simulation of any specified situation. The name was chosen during the World War II Manhattan Project because of the close connection to games based on chance and because of the location of a very famous casino in Monte Carlo [10].

Monte Carlo methods have been used for centuries, but only in the past several decades has the technique gained the status of a numerical method capable of addressing the most complex applications. Monte Carlo is now used routinely in many diverse fields, from the simulation of complex physical phenomena to ordinary daily matters.

5.1   History of Monte Carlo Method

The name and the systematic development of Monte Carlo methods dates from about 1944. There are however a number of isolated and undeveloped instances on much earlier occasions. For example, in the second half of the nineteenth century a number of people performed experiments, in which they threw a needle in a haphazard manner onto a board ruled with parallel straight lines and inferred the value of PI = 3.14... from observations of the number of intersections between needle and lines.

In 1899 Lord Rayleigh showed that a one-dimensional random walk without absorbing barriers could provide an approximate solution to a parabolic differential equation. In 1931 Kolmogorov showed the relationship between Markov stochastic processes and certain integro-differential equations.

In early part of the twentieth century, British statistical schools indulged in a fair amount of unsophisticated Monte Carlo work. Most of this seems to have been of didactic

character and rarely used for research or discovery. Only on a few rare occasions was the emphasis on original discovery rather than comforting verification. In 1908 Student (W.S. Gosset) used experimental sampling to help him towards his discovery of the distribution of the correlation coefficient.

The real use of Monte Carlo methods as a research tool stems from work on the atomic bomb during World War II. Von Neumann, Ulam and Fermi applied the method towards neutron diffusion problems in the Manhattan Project at Los Alamos. This work involved a direct simulation of the probabilistic problems concerned with random neutron diffusion in fissile material; but even at an early stage of these investigations, von Neumann and Ulam refined this particular "Russian roulette" and "splitting" methods. However, the systematic development of these ideas had to await the work of Harris and Herman Kahn in 1948. About 1948 Fermi, Metropolis, and Ulam obtained Monte Carlo estimates for the eigenvalues of Schrodinger equation.

In about 1970, the newly developing theory of computational complexity began to provide a more precise and persuasive rationale for employing the Monte Carlo method. The theory identified a class of problems for which the time to evaluate the exact solution to a problem within the class grows, at least, exponentially with M. The question to be resolved was whether or not the Monte Carlo method could estimate the solution to a problem in this intractable class to within a specified statistical accuracy in time bounded above by a polynomial in M. Numerous examples now support this contention. Karp (1985) shows this property for estimating reliability in a planar multiterminal network with randomly failing edges. Dyer (1989) establishes it for estimating the volume of a convex body in M-dimensional Euclidean space. Broder (1986) and Jerrum and Sinclair (1988) establish the property for estimating the permanent of a matrix or, equivalently, the number of perfect matchings in a bipartite graph [15].

5.2   Principles

Monte Carlo, by contrast, is the solution by probabilistic methods of nonprobabilistic problems. The distinction is somewhat useful, but often impossible to maintain. The emission of radiation from atoms and its interaction with matter is an example of a natural stochastic process since each event is to some degree unpredictable. The average behavior of such radiation can be obtained using Monte Carlo methods [7]. In most Monte Carlo applications, the physical process can be simulated directly. It only requires the system and the physical processes can be modeled from known probability density functions (pdfs). If these pdfs can be defined accurately, the simulation can be made by random sampling from the pdfs. A large number of histories (photon or electron tracks) are necessary to obtain an accurate estimate of the parameters to be calculated.
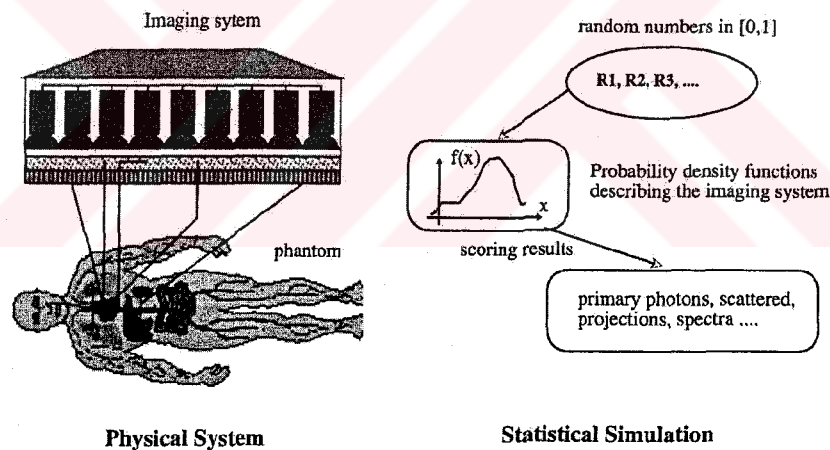
Figure 5.1 Principles of Monte Carlo simulation of an imaging system [9].

The major components of a Monte Carlo method are briefly described below. These components comprise the foundation of most Monte Carlo applications. The primary components of a Monte Carlo simulation method include the following:

- *Probability distribution functions (pdfs)* - the physical (or mathematical) system must be described by a set of pdfs.

- *Random number generator* - a source of random numbers uniformly distributed on the unit interval must be available.

- *Sampling rule* - a prescription for sampling from the specified pdf's, assuming the availability of random numbers on the unit interval, must be given.

- *Scoring (or tallying)* - the outcomes must be accumulated into overall tallies or scores for the quantities of interest.

- *Error estimation* - an estimate of the statistical error (variance) as a function of the number of trials and other quantities must be determined.

- *Variance reduction techniques* - methods for reducing the variance in the estimated solution to reduce the computational time for Monte Carlo simulation

- *Parallelization and vectorization* - algorithms to allow Monte Carlo methods to be implemented efficiently on advanced computer architectures [9].

5.2.1 Random Number Generator

A fundamental part of any Monte Carlo calculation is the random number generator, which generates uniformly distributed random numbers. Basing the numbers on detection of true random events, such as radioactive decay, can be done but this is generally very hard and time consuming. On the other hand, true random numbers cannot be calculated since they, by definition, are randomly distributed and, as a consequence of this, are unpredictable. However for practical considerations, a computer algorithm can be used to generate uniformly distributed random number from calculated seed numbers. It is the most convenient way of generating random numbers [10].

An example of an algorithm that can be used to generate uniformly distributed random numbers is the linear congruental algorithm where a series of random numbers I_n is calculated from a first seed value I_o, according to the relationship

$$I_{n+1} = (aI_n + b) \bmod (2^k) \tag{5.1}$$

where a and b are constants and k is the integer word size of the computer. If b is equal to zero then the random number generator is called a multiplicative congruental random number generator. The random numbers that are generated by such algorithms are not "true" random numbers since they are calculated from an initial starting value I_0. They are pseudo-random numbers. Pseudo-random is defined as having the appearance of randomness, but nevertheless exhibiting a specific repeatable pattern.

The sequence of random number must have some properties. The sequences of random numbers should be serially uncorrelated. The generator should not repeat, or the repetition should occur only after a long period. The sequence of random numbers should be uniform, and unbiased. They must be reproducible, and the generation of random numbers must be as fast as possible. A large number of generators are readily available, and many of these are suitable for the implementation on any computer system [16][17][18].

5.2.2   Sampling Techniques

In all Monte Carlo calculations, some information about the process to be simulated is needed. This information is expresses as probability distribution functions, pdfs, for the different processes. When simulating photon interactions, the total and partial cross-section data represent such information used to calculate the path length and interaction type. From this information, a random choice can be made on which type of interaction will occur or how far a photon will go before the next interaction.

A pdf is defined over the range of [a,b]. The function is ideally integrable so that the function can be normalized by integration over its entire range. A stochastic variable, that follows a particular pdf, can be sampled from a known frequency function $f(x)$ by the use of uniformly distributed random numbers $\mathbf{R}$ in the range 0-1. The distribution function $F(x)$ of the frequency function $f(x)$ is defined as

$$F(x) = \int_a^x f(\tau)d\tau \qquad (5.2)$$

where $a \leq x \leq b$ and τ is a dummy variable. Three different methods can be used to obtain a stochastic value x.

5.2.2.1 The distribution function method (Direct Method).

This method can be used if the inverse of the distribution function $F^{-1}(x)$ can be obtained. Since F(x) is uniformly distributed in [0-1], the sampled value of x could be obtained by substituting $F(x)$ in equation 5.2 by a uniform random number **R**, that is be $x=F^{-1}(\mathbf{R})$. An example of this method is the calculation of the photon path length. The inversion is not always possible, but in many important cases the inverse is readily obtained.

5.2.2.2 The rejection method.

This method can be used when it is too complicated to obtain the inverse of the distribution function. The method works as follows: A normalized function $f'(x) = f(x)/f_{max}(x)$ is defined where $f_{max}(x)$ is the maximum value of $f(x)$. Two uniformly distributed random numbers $\mathbf{R_1}$ and $\mathbf{R_2}$ are sampled. A stochastic variable x is calculated from the equation $x=x_{min}+\mathbf{R_1}(x_{max}-x_{min})$. If $\mathbf{R_2}$ is less than or equal to $f'(x)$ then x is accepted as sampled value, otherwise a new value of x is sampled. A typical example of using this technique is to calculate the scattering angle and photon energy after incoherent scattering.

5.2.2.3 Mixed methods.

When the distribution function method and rejection methods are impractical, the mixed method that combines the two methods can be used. Assuming the pdf can be factored as follows: $f(x)=h(x).g(x)$, where $h(x)$ is an invertible function and $g(x)$ is

relatively flat but contains most of the mathematical complexity. The method works as follows: step1. $h(x)$ is normalized producing $h'(x)$ such that

$$\int_{x_{min}}^{x_{max}} h'(x)dx = 1 \qquad (5.3)$$

step 2. $g(x)$ is normalized producing $g'(x)$ such that $g'(x) \leq 1$ for x in $[x_{min}, x_{max}]$; step 3. direct method is used to select an x using $h'(x)$ as the pdf; step 4. rejection method is applied to $g'(x)$ using the sampled value x and whether or not a random number R is less than $g'(x)$ is checked. If not, back to step 3 [10].

5.2.3 Variance Reduction Techniques (Nonanalog Sampling).

A direct Monte Carlo simulation using true probability functions may take an unacceptable long time to perform. Considering a simulation of a scintillation camera with a parallel-hole collimator. The geometrical efficiency of a low-energy, general-purpose collimator is of the order of 10^{-4}. With direct Monte Carlo simulations were applied in this case, then 9999 photons, on the average, would e rejected for each photon passing through a collimator hole, because of the small solid angle defined by the collimator holes. The calculation would therefore be very ineffective in terms of required computing time. So it is reasonable to use nonanalog sampling by introducing different types of variance reduction techniques.

In the case of the scintillation camera, a simple but effective variance-reduction technique is to simulate only photons that are emitted in directions within the solid angle Ω, which is calculated from the maximum acceptance angle θ_{max} defined by the dimensions of the collimator holes. The number of rejected photons will than be reduced significantly compared with isotropic emission. So the computing efficiency is increased.

The results obtained by nonanalog simulation are biased by the variance reduction techniques and a correction for this is required. A particle history weight, W, is introduced, which describes the probability of the particle following the current path. This weight is calculated for each particle history, and used in the calculations of results. If an event

occurs, the weight W is added to the counter rather than incrementing the counter by one unit.

There are many variance reduction techniques used in nuclear medicine [19][20][21].

5.3   Applications of the Monte Carlo Method in Nuclear Medical Imaging

5.3.1   Detector modeling

Monte Carlo simulation of detector responses and efficiencies is one of the areas, which has received considerable attention. The critical component of nuclear medicine is the scintillation detector. Increased light per gamma ray interaction, faster rise and decay times, greater stopping power and improved energy resolution are the desired characteristics. Improvements in these characteristics enable detectors to be divided into smaller elements, thus increasing resolution and minimizing dead-time losses.

5.3.2   Imaging Systems and Collimators Design

Simulation of gamma camera imaging to assess qualitatively and quantitatively the image formation process and interpretation and to assist development of collimators using deterministic methods and simplifying approximations have been developed mainly to improve speed of operation. Monte Carlo method is widely used for this purpose.

In gamma camera imaging, the choice of Collimator involves a compromise between sensitivity and spatial resolution. The relationship between sensitivity, spatial resolution and septal penetration is studied with different collimators [22]. In addition to its

quantitative clinical applications, Monte Carlo simulation may be a useful research tool for tasks such as evaluating Collimator design and optimizing gamma camera motion. Monte Carlo techniques were extensively used to analyze the performance of Collimators design for gamma camera imaging [23] Practical guidance could be offered for understanding trade-offs that must be considered for clinical imaging. Selective comparisons among different Collimators could also be presented for illustrative and teaching purposes. Approaches to the Collimator optimization problem, as well as more sophisticated "task-dependent" treatments and important considerations for Collimators design have been performed [24].

5.3.3   Image Reconstruction Algorithms

Monte Carlo simulations have been shown to be very useful for validation and comparative evaluation of image reconstruction techniques since it is possible to obtain a reference image to which reconstructed images should be compared.

5.3.4   Attenuation and Scatter Correction Techniques

The presence of scatter and attenuation in the images limits the accuracy of quantification of activity. With no corrections, the uncertainty could be as high as 50-100%. Scatter does not produce major artifacts comparable to attenuation but reduces image contrast by including a low-frequency blur in the image. The impact of scatter generally depends on the photon energy, camera energy resolution, and energy window settings, besides the object shape and the source distribution.

Monte Carlo calculations have been found to be powerful tools to quantify and correct for photon attenuation and scattering in nuclear medicine imaging since the user has the ability to separate the detected photons into their components: primary events, scatter events, etc. Monte Carlo modeling thus allows a detailed investigation of the spatial

and energy distribution of Compton scatter, which would be difficult to perform using present experimental techniques

In gamma camera imaging, simulation programs have been used to obtain information on the different processes occurring within the phantom and the detectors. For example, energy pulse-height distribution point-spread function and the scatter fraction can be obtained [25]. The scattered events in the energy-pulse-height distribution can be separated according to the number of scattering events in the phantom. The scatter fraction - the ratio between the number of scattered photons and the total number of photons - is of great importance for quantitative estimation of the scattering contribution.

5.3.5 Dosimetry and Treatment Planning

Monte Carlo calculations in the field have also been used in dosimetry modeling and computations [25].

5.3.6 Pharmacokinetic Modeling

Pharmacokinetic modeling is a useful component for the estimation of cumulated activity in various source organs in the body. There are many applications of Monte Carlo techniques have been in use in the field of pharmacokinetic modeling.

5.4 Object Model and Software Phantoms

Anthropomorphic phantoms and mathematical descriptions of human bodies are useful in radiation transport calculations. They are widely used in computer calculations of

doses delivered to the entire body and to specific organs. They are also valuable tools in the design and assessment of image reconstruction algorithms. Simple software phantoms modeled in imaging situations are in point, rod, and slab shapes of sources and attenuating media. Such simple geometries are useful in studying fundamental issues camera characteristics, scatter and attenuation. For evaluating clinically realistic distributions, a precise modeling of the human body requires appropriate information on the location, shape, density and elemental composition of the organs or tissues.

5.4.1 Object modeling

Object modeling is fundamental for performing photon and electron transport efficiently by means of a Monte Carlo method. It consists of a description of the geometry and material characteristics for an object [27][28]. The material characteristics of interest include density and energy-dependent cross-sections. The modeling includes simple geometry (SG), shape-based (SB), and voxel-based (VB) approaches. The three approaches use a piecewise uniform distribution of object characteristics to model an object. With the SG model, an object is composed of a simple combination of primitives such as cylinders and spheres. The SB approach represents the boundaries of shapes by mathematical equations. Regular shapes such as sphere, cylinder, rectangular solid, etc. have been used to approximate irregularly-shaped regions. The VB approach discretizes an object into tiny cubes (voxels) with uniform characteristics. A union of voxels of the same size represents an object.

5.4.2 Anthropomorphic Phantoms

Modeling of imaging and other medical applications is best done with phantom models that match the gross parameters of an individual patient. Computerized anthropomorphic phantoms can either be defined by mathematical (analytical) functions, or digital volume arrays. The mathematical specifications for phantoms that are available

assume a specific age, height and weight. People, however, exhibit a variety of shapes and sizes. An example for an anthropomorphic phantom is the Mathematical CArdiac Torso (MCAT) phantom, developed at the University of North Carolina [29].

5.5   Monte Carlo Computer Codes

Many Monte Carlo programs have been in use in the field of nuclear imaging with many of them available in the public domain. EGS4 [30], ITS [31], MCNP [32], SIMSET [33], SIMIND [34], MCMATV [35], PETSIM [36] are some of the Monte Carlo codes widely used.

5.5.1   SIMIND

The SIMIND code simulates a clinical scintillation camera and can easily be modified for any type of calculation or measurement encountered in gamma camera imaging. The entire code has been written in Fortran-90 and includes versions that are fully operational on VAX-VMS, most UNIX platforms and on MS-DOS. The code works as follows: photons emitted from simulated decay in the phantom are followed step by step towards the scintillation camera. SIMIND includes an accurate treatment of photon interaction in the phantom, a protecting layer and in the crystal of the detector. The simulation of back-scattering from light guides and photomultipliers is also included. Different types of collimators can be selected. The program has been shared among several groups and is a very useful research tool.

6. DESIGN OF THE INTERFACE PROGRAM

The designed user interface is based on SIMIND Monte Carlo program [34]. The interface is created with Visual Basic. Osiris imaging software [37] is used for viewing the simulated images. All these programs work in an integrated way with the interface. The interface program is a Windows based application, and is compatible with all the computer systems running Windows 98/NT/2000/XP. The general appearance of the program is shown in Figure 6.1.
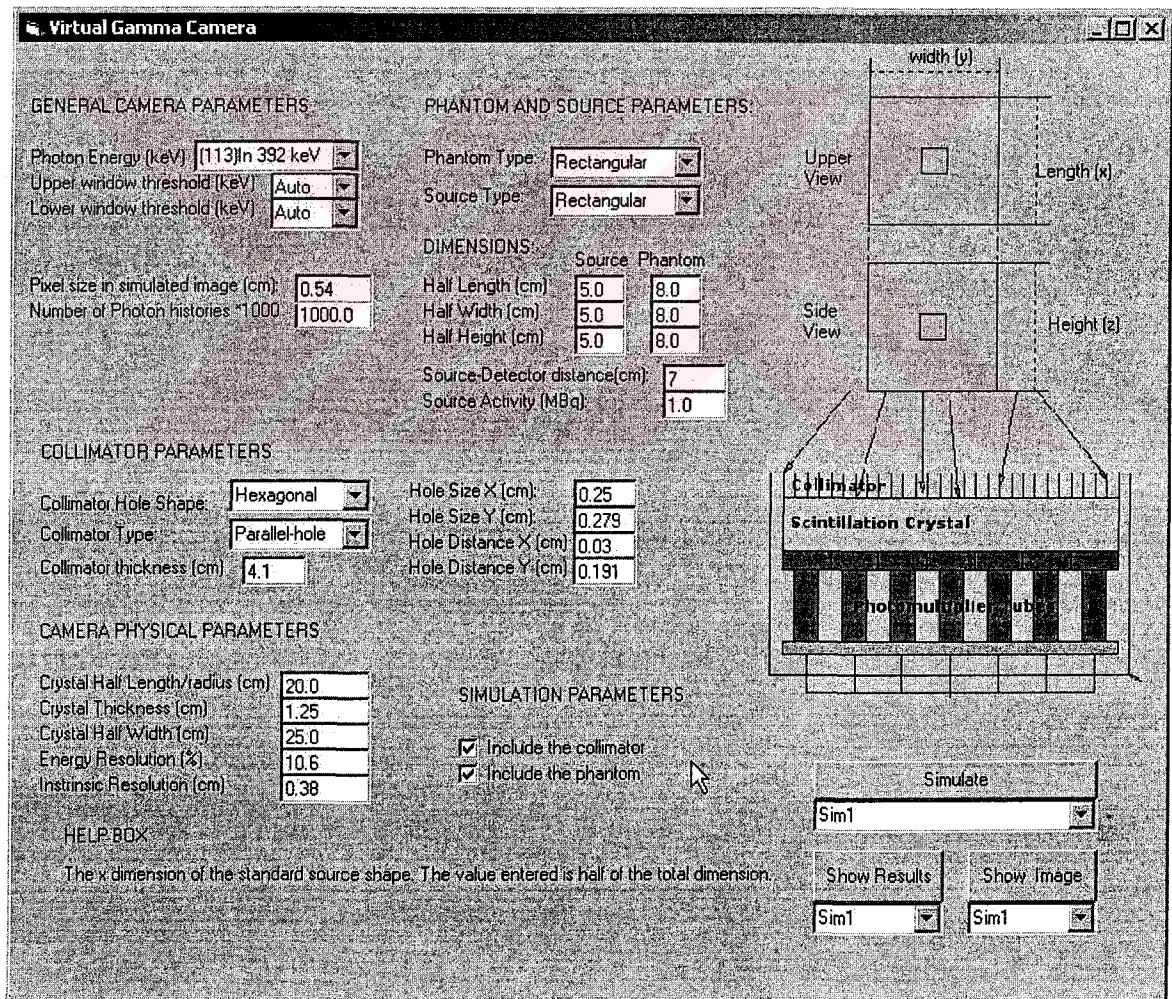

Figure 6.1 General appearance of the program.

The developed program working with SIMIND and Osiris, can perform a gamma camera simulation and create planar images of simple source and phantom geometries.

Effects of the camera characteristics and parameters on the simulated image can be studied in front of a computer. Also, the effects of parameters that cannot be measured experimentally can be studied. SIMIND has many parameters that affect the simulation of gamma camera. However, in order to make it suitable for educational purposes, only important parameters are selected, and only those can be modified through the developed interface program.

The interface is user-friendly and very simple to use. The gamma camera parameters are modified by the use of easy to access text boxes, checklists, and combo boxes. The user can define the values easily either by entering the values or selecting them from a combo list. The users can also view the simulation results and simulated images. The users can observe the differences between the results and images of different simulations performed.

6.1 Interface Layout

The gamma camera parameters are grouped as "General Parameters", "Phantom and Source parameters", "Collimator Parameters", "Camera Physical Parameters", and "Simulation Parameters". This is for easy access and helps user to understand the function of parameters. The schematic illustration of gamma camera system with the source and phantom is also included (Figure 6.1). The changes in some parameters reflect on the schematic illustration and helps the user to understand the simulation that he/she performing.

"General parameters" include photon energy, the distance between source and detector, upper and lower window thresholds, pixel size simulated image, and number of photon histories options. In "phantom and source parameters" the choices are type of phantom and source, dimensions of source and phantom, and source activity. The parameters under the group of "Collimator parameters" are the hole shape and the type of the collimator, and collimator dimensions. The parameters of "Camera Physical Parameters" include crystal dimensions, energy resolution and instrinsic resolution of the

camera. These are constant in commercial gamma cameras operating in hospitals. The last group is "simulation parameters". The selections included in this group are whether to include phantom, collimator, and cover in the simulation or not.

For performing simulations and viewing the results and the resulting images there are "Simulate", "Show Results", and "Show Image" buttons. These buttons are combined with input and output file selection combo boxes.

There is also a "Help Box" for giving information about the parameters.

6.2   Program Features

The photon energy of the radionuclide is selected from the common radionuclides used in nuclear medicine. The user can see the name and the photon energy of the radionuclide to be simulated, and select whichever she/he wants. The program simulates only the primary photons and disregards the transport of secondary electrons. The energy imparted by the electrons is assumed to be locally absorbed at the interaction site. User can also adjust the energy window by entering the upper and lower window threshold values. The values can be entered manually or automatically calculated by the program. When "auto" is selected threshold is calculated as a 20% energy window centered on the primary photon energy. The user can also define the number of photons to be simulated (number of photon histories). This parameter is directly related with the simulation time and number of detector hits during simulation. The pixel size of the resulting image can also be defined by the user. The image created can be enlarged arbitrarily by giving the proper value to the pixel size in the simulated image.

The user can choose the geometrical shape of the phantom (attenuating media) and source that is to be simulated and the distance between source and detector. There are many available source and phantom type combinations. The options for source types are ellipsoidal, rectangular, vertical cylindrical, horizontal cylindrical or point source. Available phantom choices are rectangular, horizontal cylindrical, and vertical cylindrical.

The phantom source combination chosen by user is visualized by the program. The user can see the source and phantom shape that is simulated. The user can also set the dimensions of the phantom and source by entering length, width, and height values in cm. The phantom and the source is centered in the coordinate system. The defined x, y, and z dimensions of the standard phantoms and sources are half of the total dimensions. The distance from the origin of coordinate system to the detector can be defined by entering proper value to the parameter "height to detector value" in centimeters.

User can choose whether to include the simulation of phantom or not. If the user selects to neglect the interactions in the phantom, only source specified is simulated. The activity in the source can also be defined by entering the desired value to the "source activity" parameter in (MBq). The activity of the source is used to obtain values of the detector system.

Physical dimensions of the collimator can be defined by the user. Collimator type and hole shape can be selected from several options. Parallel-hole, slant hole, converging, fan-beam, and diverging collimator type are the available for the user. The user can also select the hole shape of the specified collimator. Triangular, elliptical, hexagonal, and rectangular hole shapes are available. The user can define the thickness of the collimator, the distance between collimator holes, septal thickness and the hole dimensions in centimeters. The user can also choose from the preset collimator settings taken from the realistic, commercial collimators.

The user may also decide whether to include the collimator in the simulation or not. When collimator is not included, the photons from the source go directly to the crystal without any collimation.

The user can also change the physical properties of camera detector. The dimensions of the scintillation crystal can be specified. The thickness of the crystal can be selected from typical crystal dimensions used in nuclear medicine or it can be entered manually. Also energy resolution and intrinsic resolution of the detector can be selected from values that are determined by taking typical gamma camera performance characteristics in consider.

After entering the desired values to the camera parameters the user can perform the simulation by pressing the "simulate" button and selecting the output file from the combo box. There are also buttons for viewing the results, and viewing the simulated image file and combo file selections associated to these buttons for viewing or simulating the desired file. User can perform simulations with different parameters and selecting different output files. After performing the simulations, by pressing the "Show Results" and "Show Image" buttons and selecting the files to view by the combo boxes associated to these buttons, user can view the desired images and results and compare them. This is very useful for the user to understand how the change in parameters effect to the simulated image and to the results. The results file contains information about the simulation, and includes calculated results, which are the elapsed time of the simulation, number of detector hits, count rate of total events and window events, sensitivity, and efficiency.

There is also a help system integrated with the program. The help system provides information about all of the parameters, and simulation process. Information about the parameter is shown by bringing the mouse cursor on the desired parameter and clicking for defining new values. The description of the parameter, the possible values for the parameter, how to change a parameter, and other related information is displayed.

7. CONCLUSIONS

The goal of this thesis was to design a virtual gamma camera for educational purposes.

First, a comprehensive research has been conducted in gamma camera principles, Monte Carlo simulations and image quality. Then I created "Virtual Gamma Camera" interface software.

This software is an educational tool that works under the Windows operating system. It gives the opportunity to students and researchers, who have basic knowledge about nuclear medicine, to understand the fundamentals of gamma camera imaging. The users will be able to study virtually the effects of the camera characteristics and parameters on the simulated images and understand trade-offs that must be considered for gamma camera imaging.

This software can be used in educational institutions as part of a lab experiment. With the use of this software as a lab experiment, students will able to make gamma camera simulations and learn the fundamentals of gamma camera imaging. Students can also use the software at their home PCs in order to perform gamma camera simulations. The software is fairly user friendly. By the use of help text and program features, it is easy to make and view gamma camera simulations and study the effects of camera characteristics.

For future work, some visual improvements can be made on the designed interface. The display of simulated images can be fully integrated to the interface. More than one simulated image can be displayed on the screen. Sample simulation experiments can be added to the program. Organ phantoms should be developed for performing more realistic simulations. Finally, it should be possible to simulate SPECT camera performance.

APPENDIX A. SAMPLE SIMULATIONS

Simulation Study Number 1

In this experiment 3 simulations will be performed with the following parameters. One simulation will be performed without a collimator, one simulation with a parallel-hole collimator, and the last one with a diverging collimator. Only the source will be imaged and source is a 5x5x5cm^3 cube.

Photon energy: 140 keV (^{99}Tc^m)
Energy resolution: 10.6% at 140 keV
Source dimensions: 5x5x5cm^3
Distance from source to camera: 15 cm
Energy window: 20%

Pixel size 0.54 cm (64x64)
Crystal thickness: 0.935 (40x50 cm2)
Collimator: Hexagonal
Collimator thickness: 4 cm
Simulated photons:1000000
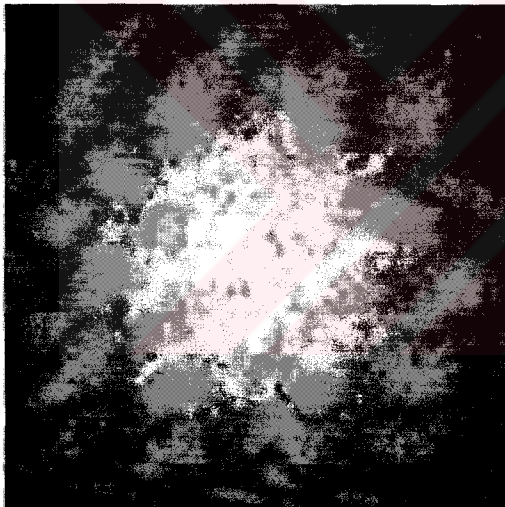
Without collimator

Results:

Detector hits: 759385
Count Rate (total events): 152878 cps
Count Rate (window events): 143112 cps
Sensitivity: 143112 cps/MBq
Sensitivity: 317710 cpm/μCi
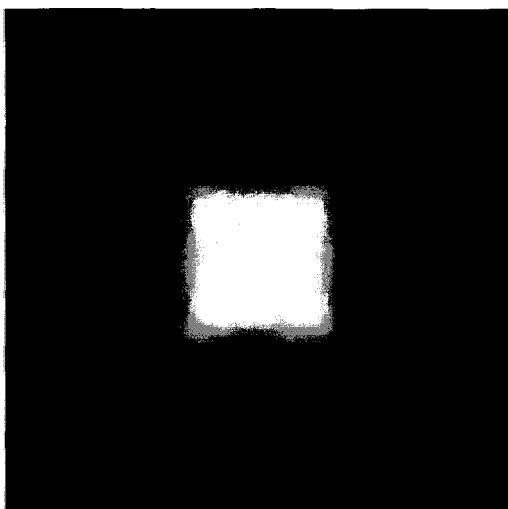
With a parallel-hole collimator

Results:

Detector hits: 885840
Count Rate (total events): 173 cps
Count Rate (window events): 160 cps
Sensitivity: 160 cps/MBq
Sensitivity: 310 cpm/μCi
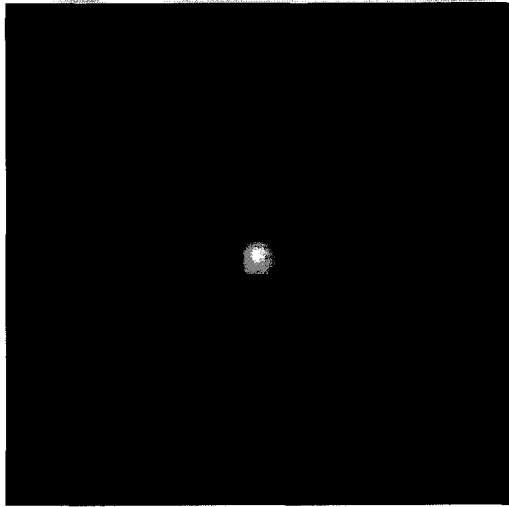
With a diverging collimator

Results:

Detector hits: 1746
Count Rate (total events): 0.30 cps
Count Rate (window events): 0.28 cps
Sensitivity: 0.28 cps/MBq
Sensitivity: 0.63 cpm/μCi

Comments:

The difference between a simulation performed without a collimator, and with a collimator can be clearly seen. In the first simulation the photons detected are covering nearly all the detector, because there is no collimation. And the count rate, thus sensitivity is very high according to other simulations. The source cannot be chosen from the image.

In the simulation with parallel-hole collimator the source is very clear. And count rates are significantly lower than the first simulation, because the photons that are not perpendicular to the crystal face are attenuated by the collimator.

In the third simulation the count rates and the size of the image is significantly small. This is because of the characteristic of the diverging collimator. The images are minified by the diverging collimator.

Simulation Study Number 2

In this experiment the effects of Compton scatter in the phantom will be studied. With two different source-phantom combinations, two simulations for each of the source-phantom combination will be performed. For each source-phantom combination one simulation including phantom, one simulation without phantom will be performed with the following parameters.

Photon energy: 140 keV (^{99}Tc^m)
Energy resolution: 10.6% at 140 keV
Source dimensions: 7x7x5cm
Phantom dimensions: 12x12x12
Distance from source to camera: 5 cm
Energy window: 20%

Pixel size 0.54 cm (64x64)
Crystal thickness: 0.935 (40x50 cm2)
Collimator: Hexagonal
Collimator thickness: 4 cm
Simulated photons:1000000
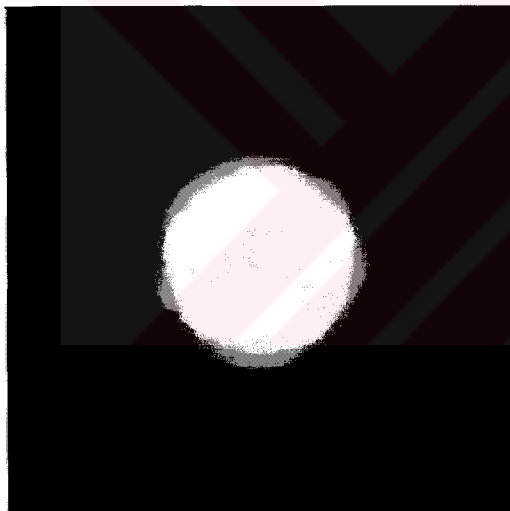
Source: Vertical cylindrical (7x7x5cm)

Phantom: not included

Results:

Detector hits: 885981
Count Rate (total events): 173 cps
Count Rate (window events): 160 cps
Sensitivity: 160 cps/MBq
Sensitivity: 356 cpm/μCi
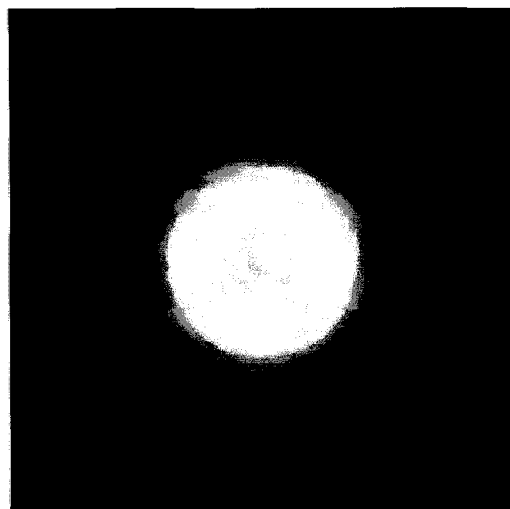
Source: Vertical cylindrical (7x7x5cm)

Phantom: Rectangular (12x12x12cm)

Results:

Detector hits: 885754
Count Rate (total events): 105 cps
Count Rate (window events): 46 cps
Sensitivity: 46 cps/MBq
Sensitivity: 102 cpm/μCi
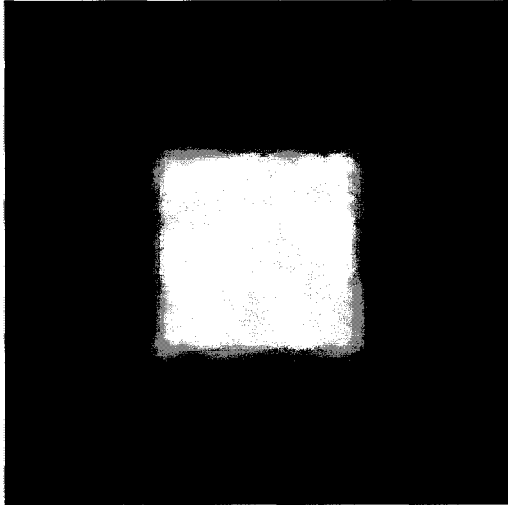
Source: Rectangular (7x7x5cm)

Phantom: not included

<u>**Results:**</u>

Detector hits: 886093
Count Rate (total events): 173 cps
Count Rate (window events): 160 cps
Sensitivity: 160 cps/MBq
Sensitivity: 356 cpm/μCi
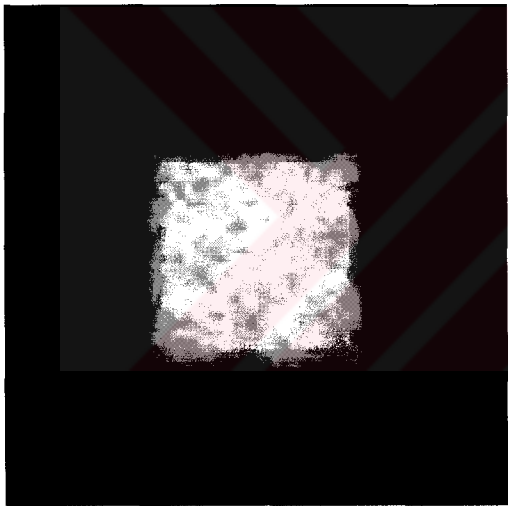
Source: Rectangular (7x7x5cm)

Phantom: Ver. Cylindrical (12x12x12cm)

<u>**Results:**</u>

Detector hits: 885669
Count Rate (total events): 44 cps
Count Rate (window events): 42cps
Sensitivity: 22 cps/MBq
Sensitivity: 49 cpm/μCi

Comments:

It is obvious that in the simulations including phantoms the count rate, thus the sensitivity decreases dramatically. This is because of the Compton interactions occurring within the phantom. This scattering prevents photons reaching the crystal. Also the window and total event rate decreases with the inclusion of phantom. This is because the photons reaching the detector lose energy in the phantom. They are not counted in the energy window and disregarded. The resolution decreases obviously by the inclusion of a phantom causing scatter. The difference between the images is clearer in the simulation with a rectangular source and a cylindrical phantom.

Simulation Study Number 3

In this simulation study, the effect of the energy window to the resulting image, sensitivity and resolution will be shown. 4 simulations will be performed with different energy windows (40%, 20%, 10%, 5%) without changing the source and phantom shape and dimensions.

Photon energy: 140 keV ($^{99}Tc^{m}$)
Energy resolution: 10.6% at 140 keV
Source dimensions: 5x5x5cm (sphere)
Phantom dimensions: 9x9x9cm (rect.)
Distance from phantom to camera: 6 cm

Pixel size 0.54 cm (64x64)
Crystal thickness: 0.935 (40x50 cm2)
Collimator: Hexagonal
Collimator thickness: 4 cm
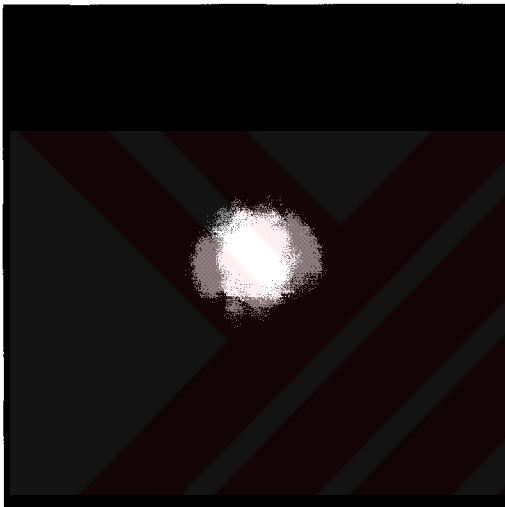
Energy Window: %40
Upper win. Threshold: 168 keV
Lower win. Threshold: 112 keV

Results:

Detector hits: 885739
Count Rate (total events): 136 cps
Count Rate (window events): 83 cps
Sensitivity: 83 cps/MBq
Sensitivity: 186 cpm/μCi
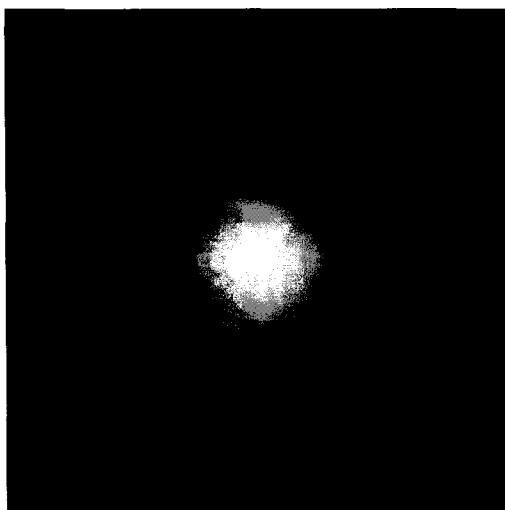
Energy Window: %20
**Upper win. Threshold:** 154 keV
Lower win. Threshold: 126 keV

Results:

Detector hits: 886180
Count Rate (total events): 135 cps
Count Rate (window events): 64 cps
Sensitivity: 64 cps/MBq
Sensitivity: 142 cpm/μCi
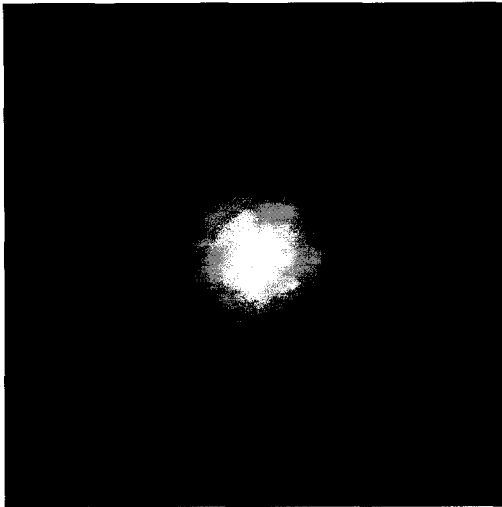
Energy Window: %10
Upper win. Threshold: 147 keV
Lower win. Threshold: 133 keV

Results:

Detector hits: 885504
Count Rate (total events): 136 cps
Count Rate (window events): 43 cps
Sensitivity: 43 cps/MBq
Sensitivity: 95 cpm/μCi

Energy Window: %5
Upper win. Threshold: 143.5 keV
Lower win. Threshold: 136.5 keV

Results:

Detector hits: 885106
Count Rate (total events): 135 cps
Count Rate (window events): 23 cps
Sensitivity: 23 cps/MBq
Sensitivity: 53 cpm/μCi

Comments:

The sensitivity decreases dramatically by the decrease in the energy window. The corresponding sensitivities are 83 cps/MBq for 40% energy window; 54 cps/MBq for 20% energy window; 43 cps/MBq for 10% energy window, and 23 cps/MBq for 5% energy window. The reason for this is that when the energy window decreases, the photons striking the crystal in the energy window decreases, and this results in the loss of sensitivity. There is no obvious difference in the images.

Simulation Study Number 4

In this simulation study, the effect of the collimator thickness on the resulting image, and sensitivity will be simulated. 4 simulations will be performed with different collimator thickness (10 cm, 7 cm, 4 cm, and 1 cm) without changing the source and phantom shape and dimensions.

Photon energy: 140 keV (^{99}Tc^m)
Energy resolution: 10.6% at 140 keV
Source dimensions: 5x5x5cm (rect)
Phantom dimensions: 9x9x9cm (ver.cyl.)

Distance from phantom to camera: 5 cm
Pixel size 0.54 cm (64x64)
Crystal thickness: 0.935 (40x50 cm2)
Collimator: Hexagonal, Parallel-hole
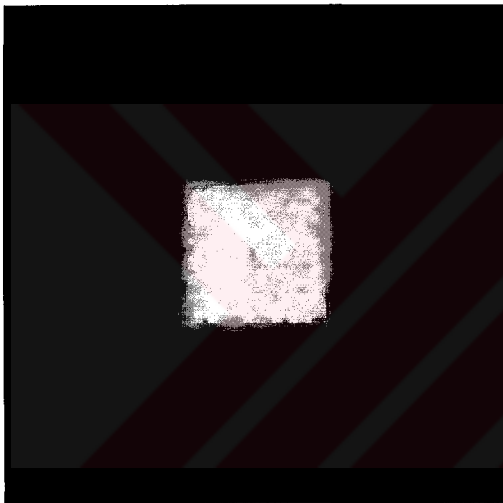
Collimator Thickness: 10 cm

Results:

Detector hits: 885165
Count Rate (total events): 9.4 cps
Count Rate (window events): 4.8 cps
Sensitivity: 4.8 cps/MBq
Sensitivity: 10.72 cpm/μCi
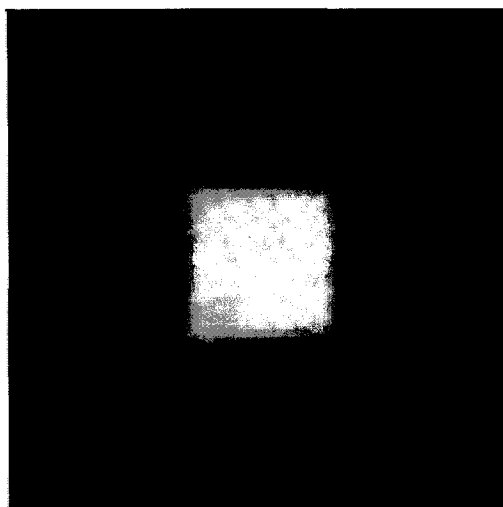
Collimator Thickness: 7 cm

Results:

Detector hits: 885527
Count Rate (total events): 19.3 cps
Count Rate (window events): 9.8 cps
Sensitivity: 9.8 cps/MBq
Sensitivity: 21.8 cpm/μCi
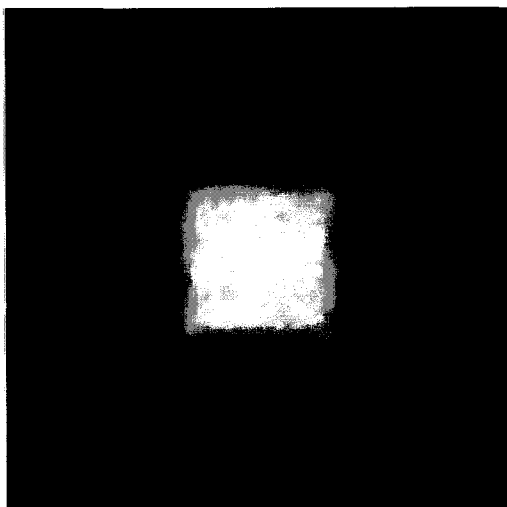
Collimator Thickness: 4 cm

<u>Results:</u>

Detector hits: 885323
Count Rate (total events): 59.3 cps
Count Rate (window events): 30.4 cps
Sensitivity: 30.4 cps/MBq
Sensitivity: 67.5 cpm/μCi

Collimator Thickness: 1 cm

<u>Results:</u>

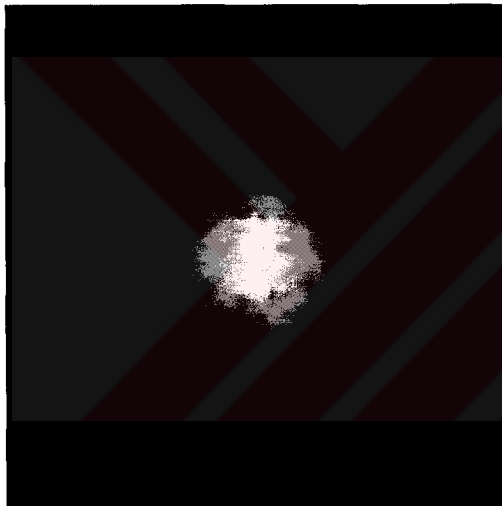Detector hits: 891494
Count Rate (total events): 926 cps
Count Rate (window events): 472 cps
Sensitivity: 472 cps/MBq
Sensitivity: 2048 cpm/μCi

**Comments:**

The effect of collimator thickness is clearly shown with this experiment. The sensitivity increases with the decrease in the collimator length. On the other hand the resolution decreases by the increase in the sensitivity. It can be clearly seen in the resulting images. In the image with 1 cm collimator thickness, the resolution is very poor and image is distorted.

With a longer collimator thickness, most photons are attenuated, except those exactly perpendicular to the crystal face. This increase in selectivity increases the resolution and decreases the count rate. Shortening the length allows more photons to reach the crystal; thus the count rate is higher. The spatial resolution however is decreased because the photons coming through a hole in the collimator are from a larger area.

APPENDIX B. USER MANUAL

What is Virtual Gamma Camera?

This is a computer program that simulates a real gamma camera. It is created for educational purposes. One can create planar images of simple source and phantom geometries and understand the fundamentals of gamma cameras. And it is possible to change various gamma parameters and see the effects on the simulated image, and compare the results.
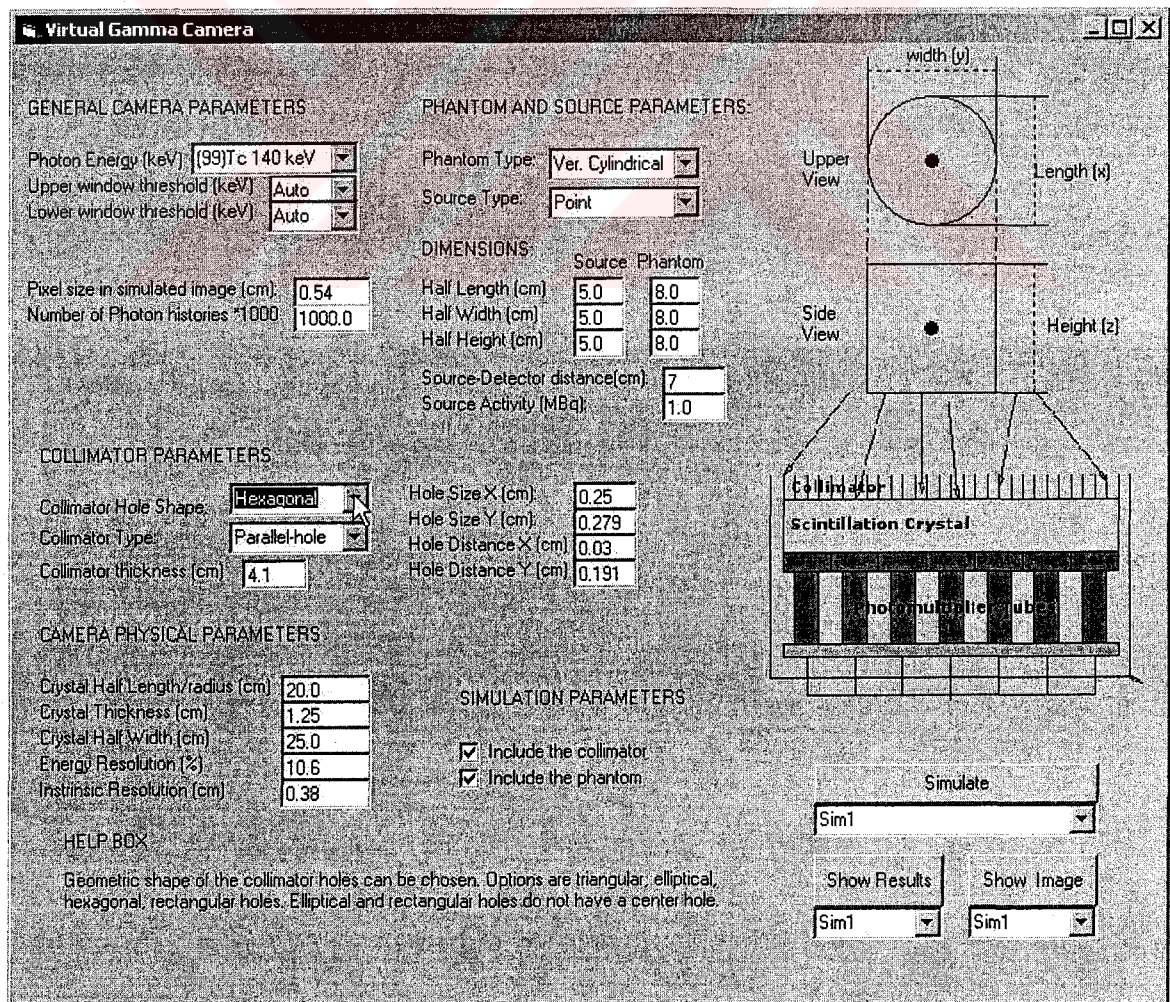
Layout of Virtual Gamma Camera

Gamma Camera Parameters

The parameters that can be changed by the user and their explanations are as follows:

Phantom Type

The type of phantom that is to be simulated. Available standard phantoms are: rectangular, vertical cylindrical, horizontal cylindrical.

Source Type

The type of source distribution that is to be simulated. Available standard source shapes are: ellipsoidal, rectangular, vertical cylindrical, horizontal cylindrical, or point source.

Collimator Shape

Geometric shape of the collimator holes can be chosen. Options are triangular, elliptical, hexagonal, rectangular holes. Elliptical and rectangular holes do not have a center hole.

Collimator Type

The type of the collimator used in simulation is defined here. The possible options are; Parallel-hole, Slant hole, Converging, Fan-beam, and diverging collimator.

Upper window threshold [keV]

The value of upper energy window. The value can be entered manually or auto can be chosen. In auto mode (if auto mode is selected in upper or lower energy window), threshold is calculated as a 20% energy window centered on the primary photon energy.

Lower Window Threshold [keV]

The value of lower energy window. The value can be entered manually or auto can be chosen. In auto mode (if auto mode is selected in upper or lower energy window), threshold is calculated as a 20% energy window centered on the primary photon energy [keV].

Crystal Half Length/Radius [cm]

The length of cylindrical crystal in x-direction. If "Crystal Half Width" is equal to zero, then the detector is assumed to be a cylinder, and the radius of the cylinder is defined by this parameter. Crystal may be 25 to 66 cm in diameter. Remember you are entering half of the actual value.

Crystal Thickness [cm]

The thickness of the scintillation crystal. The thickness of crystal generally changes between 0.635 cm and 1.5 cm. Most common crystal thickness is 0.935 cm and 1.25 cm.

Crystal Half Width [cm]

The half of the total width of the detector. If this parameter is equal to zero, than the detector is assumed to be a cylinder with a radius equal to 'Crystal Half Length/radius'. The Crystal may be 25 to 66 cm in diameter. Remember you are entering half of the actual value.

Source-Detector Distance [cm]

The distance from the origin of the coordinate system to the lowest part of the detector. This value is added to phantom height and actual distance from origin to detector is calculated.

Number of Photon Histories *1000

This parameter represents the number of photon histories that are simulated. The value is multiplied by 1000. This value is directly related to the number of counts, thus the duration of the simulation.

Hole Size X [cm]

The length of the collimator hole in the x-direction [cm].

Hole Size Y [cm]

The length of the collimator hole in the y-direction. This value is also known as the inner hole diameter [cm].

Hole Distance X [cm]

The distance between two collimator holes in the x-direction [cm].

Hole Distance Y [cm]

The distance between two collimator holes in the y-direction. This value is also known as the septal thickness [cm].

Collimator Thickness [cm]

The physical thickness of the collimator [cm].

Energy Resolution [%]

The energy resolution of the detector. This value is between 10% and 15% in real cameras. The less the resolution, the better the image quality.

Instrinsic Resolution [cm]

The instrinsic spatial resolution of the crystal. This value is varies from 3cm to 6 cm in real cameras. It is better to have a smaller instrinsic resolution.

Source Activity [MBq]

The activity of the source. It is used to obtain correct values of the sensitivity and different calculated count rates. It does not decide the number of photons that are actually are simulated [MBq].

Photon energy [keV]

The energy of the photon. You can select from one of the common radionuclides listed.

Pixel Size

The pixel size is used to define the area on the crystal that is represented by the image. The image created can be zoomed in or enlarged arbitrarily by giving the proper value of the pixel size. The value must be bigger than zero.

Include the collimator (checkbox)

Include simulation of scintillation camera collimator, or not.

Include the phantom (checkbox)

Include the simulation of phantom or not.

Source Dimensions Half Length, Half Width, Half Height [cm]

The x, y, and, z dimensions of the standard source shapes. The values entered are half of the total dimensions.

Phantom Dimensions Half Length, Half Width, Half Height [cm]

The x, y, and, z dimensions of the standard phantoms. The values entered are half of the total dimensions.

How To Use The Program?

How to Modify Parameters?

The parameters can be modified either entering the textboxes beside the parameters or selecting from the combo box. The simulations parameters are checkboxes and they are changed by clicking on the checkboxes.

How to Make a Simulation?

After making the changes in desired parameters, the program is ready to perform a simulation. First, you must select the simulation file name from the combo box below the "Simulate" button. Then start the simulation by pushing the "Simulate" button.

How to View the Results File?

In order to view the results of the related simulation, select the simulation file name that you want to observe and click the "Results" button. In other words you must choose results of which simulation file (sim1, sim2, or sim3) you want to see before clicking the button. The Results file is shown as a pop-up. Note: You must perform the simulation before trying to view the results.

How to View the Resulting Image?

To view the image, you must choose the simulation file to open by choosing from the combo box below "Show Image" button. Then by clicking the "Show Image" button the raw data dialog appears. Like viewing the results file you must perform the related simulation before trying to view the image. 16Bits/pixel depth must be selected and then by clicking the guess button the width and height of the image in pixels are appeared. Then by clicking "OK" button the resulting image can be viewed.

Note: It is important to select 16 Bits/pixel depth before clicking the guess button. Otherwise the image cannot be displayed correctly.
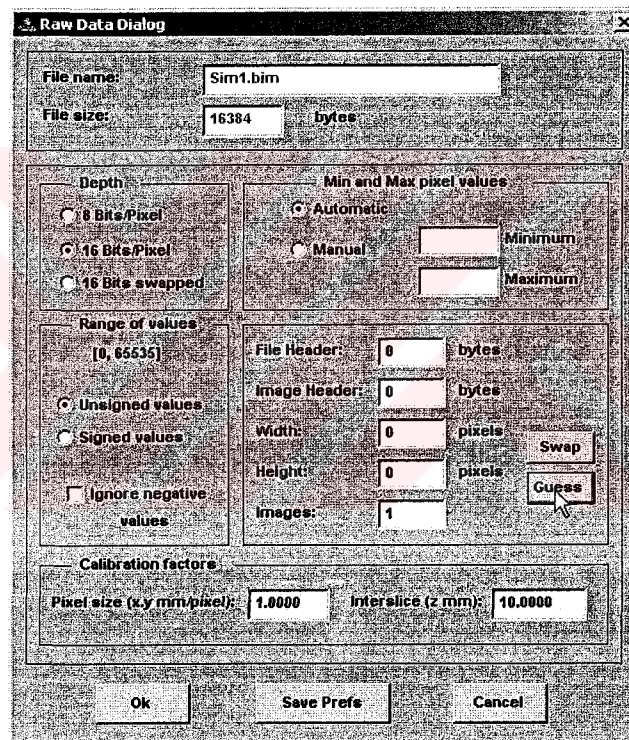
Viewing the image.

How to Get Help?

When the mouse cursor is brought on the desired parameter and clicked for defining new values, information about the parameter is shown on the help screen. The description of the parameter, the possible values for the parameter, how to change a parameter, and other related information is displayed.

APPENDIX C. EXPERIMENT HANDOUT

GAMMA CAMERA SIMULATION

OBJECT

The objective of this experiment is to simulate gamma camera and observe the effects of gamma characteristics.

EQUIPMENT

1- A computer
2- Virtual Gamma Camera software package

THEORY

Nuclear medicine is a medical specialty that uses safe, painless, and cost-effective techniques both to image the body and treat disease. Nuclear medicine imaging is unique in that it documents organ function and structure, in contrast to diagnostic radiology, which is based upon anatomy. It is a way to gather medical information that may otherwise be unavailable, require surgery, or necessitate more expensive diagnostic tests.

Nuclear medicine uses very small amounts of radioactive materials or radiopharmaceuticals to diagnose and treat disease. Radiopharmaceuticals are substances that are attracted to specific organs, bones, or tissues. The radiopharmaceuticals used in nuclear medicine emit gamma rays that can be detected externally by gamma or PET cameras. These cameras work in conjunction with computers used to form images that provide data and information about the area of body being imaged.

Gamma Camera

The scintillation camera is the most commonly uses imaging system in nuclear medicine today for both planar and tomographic studies. The basic components of a gamma camera imaging system are the collimator, the scintillation crystal (detector), an array of photomultiplier tubes, a pulse height analyzer (PHA), and a cathode ray tube for displaying images.
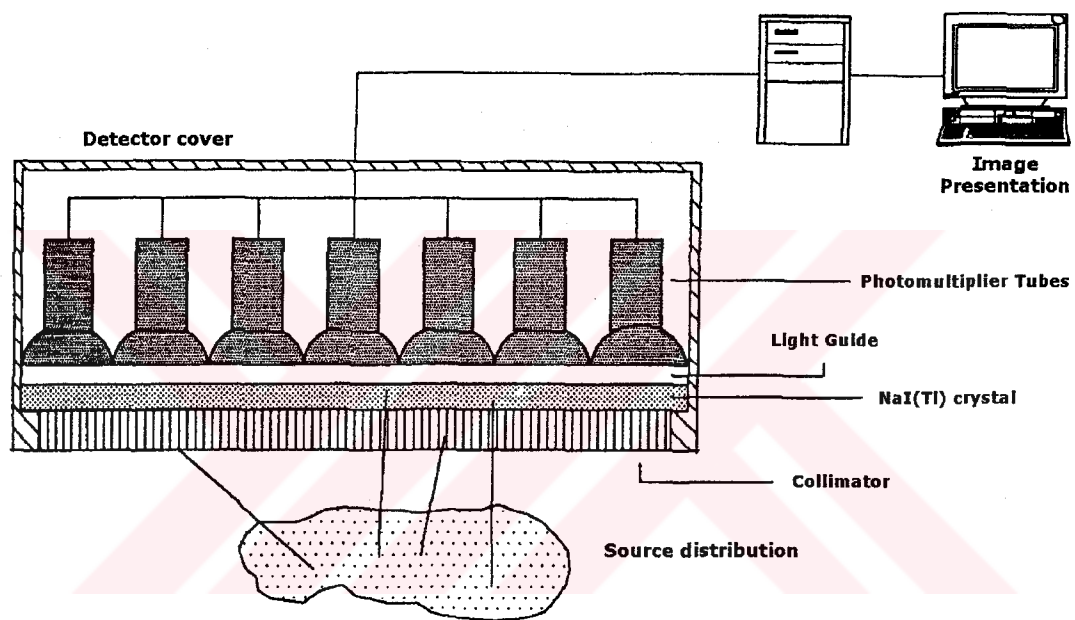
A schematic illustration of gamma camera.

A gamma camera, converts photons emitted by the radionuclide in the patient into a light pulse and subsequently into a voltage signal. This signal is used to form an image of the distribution of the radionuclide.

Photons emitted from the activity distribution in the patient are projected through the collimator onto the sodium iodine crystal, where they interact and create scintillation light. The light is detected by photomultiplier tubes (PMTs), and transformed into current pulses, proportional to the flux of the incoming photons. These pulses are processed by analogue and/or digital electronic circuits, and computation with suitable algorithms results in output signals (data) representing the scintillation light distribution created in the crystal, and the energy deposited in the crystal.

PROCEDURE

Make the following simulations using the computer program.

1-   Enter the following parameters to the program. Make a simulation with and without a collimator. Compare the images and observe the results (sensitivity, count rate).

> Photon energy: 140 keV (^{99m}Tc)
> Energy resolution: 10.6% at 140 keV
> Source dimensions: 5x5x5cm rectangular sauce
> Distance from source to camera: 15 cm
> Energy window: 20% (auto)
> Pixel size 0.54 cm (64x64)
> Crystal thickness: 0.935 (40x50 cm2)
> Collimator: Hexagonal
> Collimator thickness: 4 cm
> Simulated photons: 1000000

2-   Enter the following parameters to the program. Make one simulation including phantom, and one simulation without a phantom. Compare the images and observe the results (sensitivity, count rate).

> Photon energy: 140 keV (^{99m}Tc)
> Energy resolution: 10.6% at 140 keV
> Source dimensions: 7x7x5cm rectangular
> Phantom dimensions: 12x12x12 rectangular
> Distance from source to camera: 5 cm
> Energy window: 20%
> Pixel size 0.54 cm (64x64)
> Crystal thickness: 0.935 (40x50 cm2)
> Collimator: Hexagonal
> Collimator thickness: 4 cm
> Simulated photons: 1000000

3-   Enter the following parameters to the program. Make 4 simulations with different collimator thickness (5cm, 3cm, 2cm, 1cm). Compare the images and observe the results (sensitivity, count rate).

> Photon energy: 140 keV (^{99m}Tc)
> Energy resolution: 10.6% at 140 keV
> Source dimensions: 5x5x5cm (rectangular)
> Phantom dimensions: 9x9x9cm (vertical cylindrical.)
> Distance from phantom to camera: 5 cm
> Pixel size 0.54 cm (64x64)
> Crystal thickness: 0.935 (40x50 cm2)
> Collimator: Hexagonal, Parallel-hole

Questions

1- Present your simulation results. Make comments about the simulations.

2- Explain the terms sensitivity, resolution. Discuss the trade-off between sensitivity and resolution in gamma camera imaging.

3- Explain the types of collimators briefly.

4- Discuss the effect of septal length of collimator on sensitivity and resolution.

APPENDIX D. PROGRAM SOURCE CODE

Form1

```
Private Sub Check1_GotFocus(Index As Integer)
    Label1 = "Include simulation of scintillation camera collimator, or not. " & "-Include the
simulation of phantom or not."
End Sub


Private Sub Combo1_GotFocus()
    Label1 = "The type of Phantom that is to be simulated. Available standard phantoms are:
Rectangular, Vertical Cylindrical, Horizontal Cylindrical."
End Sub


Private Sub Combo3_GotFocus()
    Label1 = "The type of source distribution that is to be simulated. Available standart
source shapes are: Ellipsoidal, Rectangular, Vertical Cylindrical, Horizontal Cylindirical,
or Point source."
End Sub


Private Sub Combo4_GotFocus()
    Label1 = "Geometric shape of the collimator holes can be chosen. Options are
triangular, elliptical, hexagonal, rectangular holes. Elliptical and rectangular holes do not
have a center hole."
End Sub


Private Sub Combo5_GotFocus()
Label1 = "The type of the collimator used in simulation is defined here. The possible
options are; Parallel-hole, Slant hole, Converging, Fan-beam, and diverging collimator."
End Sub


Private Sub Combo8_GotFocus()
Label1 = "The value of upper energy window. The value can be entered manually or auto
can be chosen. In auto mode (if auto mode is selected in upper or lower energy window),
threshold is calculated as a 20% energy window centered on the primary photon energy."
End Sub


Private Sub Combo9_GotFocus()
    Label1 = "The value of lower energy window. The value can be entered manually or
auto can be chosen. In auto mode (if auto mode is selected in upper or lower energy
window), threshold is calculated as a 20% energy window centered on the primary photon
energy."
End Sub


Private Sub Command1_Click()
Dim FileName  As String
Dim FileName1 As String
Dim Temp As String
```

```
Dim isim As String

Dim Temp1 As String
Dim X As Integer

    FileName = App.Path & "\simind.smc"
    FileName1 = App.Path & "\simind.tmp"

    Open FileName For Input As #1
    Open FileName1 For Output As #2

    X = 1

    Do Until EOF(1)
        Line Input #1, Temp

        Select Case X
            Case 2
                Temp1 = Text1.Text & Space(11 - Len(Text1.Text))
                Temp1 = Temp1 & Text2.Text & Space(11 - Len(Text2.Text))
                Temp1 = Temp1 & Text3.Text & Space(11 - Len(Text3.Text))
                Temp1 = Temp1 & Text4.Text & Space(11 - Len(Text4.Text))
                Temp1 = Temp1 & Text5.Text & Space(11 - Len(Text5.Text))
                Temp1 = Temp1 & " " & Text6.Text & Space(8 - Len(Text6.Text))
                Temp1 = Temp1 & Text7.Text & Space(11 - Len(Text7.Text))
                Temp1 = Temp1 & Text8.Text & Space(11 - Len(Text8.Text))
                Print #2, Temp1

            Case 4
                Temp1 = ""
                For Y = 0 To 14
                    'If Not y = 1 Then
                        Temp1 = Temp1 & IIf(Check1(Y).Value = 1, " T", " F")
                    'End If
                Next
                Temp1 = Temp1 & Mid(Temp, 31, Len(Temp))
                Print #2, Temp1

            Case 6
                Temp1 = ""

                Select Case Combo10.Text
                    Case "(125)I 35 keV"
                        Text9.Text = 35
                    Case "(201)Tl 77 keV"
                        Text9.Text = 77
                    Case "(133)Xn 81 keV"
                        Text9.Text = 81
                    Case "(67)Ga 93 keV"
```

```
                Text9.Text = 93
            Case "(57)Co 122 keV"
                Text9.Text = 122
            Case "(99)Tc 140 keV"
                Text9.Text = 140
            Case "(123)I 159 keV"
                Text9.Text = 159
            Case "(113)In 392 keV"
                Text9.Text = 392
            Case Else
                Text9.Text = Combo10.Text
        End Select


        Temp1   =   Space(12   -   Len(Format(CDbl(Text9.Text),   "0.0###")))   &
Format(CDbl(Text9.Text), "0.0###")
        Temp1 = Temp1 & Space(12 - Len(Format(CDbl(Text10.Text), "0.0###"))) &
Format(CDbl(Text10.Text), "0.0###")
        Temp1 = Temp1 & Space(12 - Len(Format(CDbl(Text11.Text), "0.0###"))) &
Format(CDbl(Text11.Text), "0.0###")
        Temp1 = Temp1 & Space(12 - Len(Format(CDbl(Text12.Text), "0.0###"))) &
Format(CDbl(Text12.Text), "0.0###")
        Temp1 = Temp1 & Space(12 - Len(Format(CDbl(Text13.Text), "0.0###"))) &
Format(CDbl(Text13.Text), "0.0###")


        Print #2, Temp1


    Case 7
        Temp1 = ""


        Temp1   =   Space(12   -   Len(Format(CDbl(Text14.Text),   "0.0###")))   &
Format(CDbl(Text14.Text), "0.0###")
        Temp1 = Temp1 & Space(12 - Len(Format(CDbl(Text15.Text), "0.0###"))) &
Format(CDbl(Text15.Text), "0.0###")
        Temp1 = Temp1 & Space(12 - Len(Format(CDbl(Text16.Text), "0.0###"))) &
Format(CDbl(Text16.Text), "0.0###")
        Temp1 = Temp1 & Space(12 - Len(Format(CDbl(Text17.Text), "0.0###"))) &
Format(CDbl(Text17.Text), "0.0###")
        Temp1 = Temp1 & Space(12 - Len(Format(CDbl(Text18.Text), "0.0###"))) &
Format(CDbl(Text18.Text), "0.0###")


        Print #2, Temp1


    Case 8
        Temp1 = ""


        Temp1 = Mid(Temp, 1, 12)
        Temp1 = Temp1 & Space(12 - Len(Format(CDbl(0 - Text19.Text), "0.0###")))
& Format(CDbl(0 - Text19.Text), "0.0###")
        Temp1 = Temp1 & Mid(Temp, 25, 12)
```

```
Select Case Combo1.Text
   Case "Rectangular"
      ptype = 2
   Case "Ver. Cylindrical"
      ptype = 3
   Case "Hor. Cylindrical"
      ptype = 4
   Case Else
      ptype = Combo1.Text
   End Select

Temp1 = Temp1 & Space(12 - Len(Format(CDbl(ptype), "0.0###"))) &
Format(CDbl(ptype), "0.0###")

   Select Case Combo3.Text
   Case "Ellipsoidal"
      stype = 1
   Case "Rectangular"
      stype = 2
   Case "Ver. Cylindrical"
      stype = 3
   Case "Hor. Cylindrical"
      stype = 4
   Case "Point"
      stype = 5
   Case Else
      stype = Combo3.Text
End Select

Temp1 = Temp1 & Space(12 - Len(Format(CDbl(stype), "0.0###"))) &
Format(CDbl(stype), "0.0###")

   Print #2, Temp1

Case 9
   Temp1 = ""

Temp1 = Mid(Temp, 1, 36)
Temp1 = Temp1 & Space(12 - Len(Format(CDbl(Text22.Text), "0.0###"))) &
Format(CDbl(Text22.Text), "0.0###")

   Select Case Combo8.Text
   Case "Auto"
      Text23.Text = -20
   Case Else
      Text23.Text = Combo8.Text
End Select
```

```
        Temp1 = Temp1 & Space(12 - Len(Format(CDbl(Text23.Text), "0.0###"))) &
Format(CDbl(Text23.Text), "0.0###")

        Print #2, Temp1

    Case 10
        Temp1 = ""

        'Temp1 = Temp1 & Space(12 - Len(Format(CDbl(Text24.Text), "0.0###"))) &
Format(CDbl(Text24.Text), "0.0###")
        'Temp1 = Temp1 & Mid(Temp, 13, Len(Temp))
        Select Case Combo9.Text
            Case "Auto"
                Text24.Text = -20
            Case Else
                Text24.Text = Combo9.Text
        End Select
        Temp1  =  Space(12  -  Len(Format(CDbl(Text24.Text),  "0.0###")))  &
Format(CDbl(Text24.Text), "0.0###")
        Temp1 = Temp1 & Space(12 - Len(Format(CDbl(Text38.Text), "0.0###"))) &
Format(CDbl(Text38.Text), "0.0###")
        Temp1 = Temp1 & Space(12 - Len(Format(CDbl(Text39.Text), "0.0###"))) &
Format(CDbl(Text39.Text), "0.0###")
        Temp1 = Temp1 & Space(12 - Len(Format(CDbl(Text40.Text), "0.0###"))) &
Format(CDbl(Text40.Text), "0.0###")
        Temp1 = Temp1 & Space(12 - Len(Format(CDbl(Text41.Text), "0.0###"))) &
Format(CDbl(Text41.Text), "0.0###")

        Print #2, Temp1

    Case 11
        Temp1 = ""

        Temp1  =  Space(12  -  Len(Format(CDbl(Text25.Text),  "0.0###")))  &
Format(CDbl(Text25.Text), "0.0###")
        Temp1 = Temp1 & Mid(Temp, 13, 12)
        Temp1 = Temp1 & Space(12 - Len(Format(CDbl(Text26.Text), "0.0###"))) &
Format(CDbl(Text26.Text), "0.0###")
        Temp1 = Temp1 & Space(12 - Len(Format(CDbl(Text27.Text), "0.0###"))) &
Format(CDbl(Text27.Text), "0.0###")
        Temp1 = Temp1 & Space(12 - Len(Format(CDbl(Text28.Text), "0.0###"))) &
Format(CDbl(Text28.Text), "0.0###")

        Print #2, Temp1

    Case 15
        Temp1 = ""
```

```
        Temp1  =  Space(12  -  Len(Format(CDbl(Text29.Text),  "0.0###")))  &
Format(CDbl(Text29.Text), "0.0###")
        Temp1 = Temp1 & Space(12 - Len(Format(CDbl(Text30.Text), "0.0###"))) &
Format(CDbl(Text30.Text), "0.0###")
        Temp1 = Temp1 & Space(12 - Len(Format(CDbl(Text31.Text), "0.0###"))) &
Format(CDbl(Text31.Text), "0.0###")
        Temp1 = Temp1 & Space(12 - Len(Format(CDbl(Text32.Text), "0.0###"))) &
Format(CDbl(Text32.Text), "0.0###")
        Temp1 = Temp1 & Mid(Temp, 49, 12)

        Print #2, Temp1

    Case 16
        Temp1 = ""

        Temp1 = Mid(Temp, 1, 12)
        Temp1 = Temp1 & Space(12 - Len(Format(CDbl(Text33.Text), "0.0###"))) &
Format(CDbl(Text33.Text), "0.0###")
        Temp1 = Temp1 & Mid(Temp, 25, 12)
        Select Case Combo4.Text
            Case "Triangular"
                colshape = 1
            Case "Elliptical"
                colshape = 2
            Case "Hexagonal"
                colshape = 3
            Case "Rectangular"
                colshape = 4
            Case Else
                colshape = Combo4.Text
            End Select
        Temp1 = Temp1 & Space(12 - Len(Format(CDbl(colshape), "0.0###"))) &
Format(CDbl(colshape), "0.0###")

        Select Case Combo5.Text
            Case "Parallel-hole"
                coltype = 0
            Case "Slant hole"
                coltype = 1
            Case "Converging"
                coltype = 2
            Case "Fan-beam"
                coltype = 3
            Case "Diverging"
                coltype = 4
            Case Else
                coltype = Combo5.Text
            End Select
```

```
        Temp1 = Temp1 & Space(12 - Len(Format(CDbl(coltype), "0.0###"))) &
Format(CDbl(coltype), "0.0###")

        Print #2, Temp1

    Case 21
      Temp1 = ""

        Temp1 = Temp1 & Space(12 - Len(Format(CDbl(Text36.Text), "0.0###"))) &
Format(CDbl(Text36.Text), "0.0###")
        Temp1 = Temp1 & Space(12 - Len(Format(CDbl(Text37.Text), "0.0###"))) &
Format(CDbl(Text37.Text), "0.0###")
        Temp1 = Temp1 & Mid(Temp, 25, Len(Temp))

        Print #2, Temp1

    Case Else
        Print #2, Temp
    End Select

    X = X + 1
Loop

Close

Kill FileName
Name FileName1 As FileName

isim = Text42
Dim RetVal

RetVal = Shell(App.Path & "\simind simind " & Combo2.Text, 1)

End Sub

Private Sub Command2_Click()
    Form2.Show
    RetVal = Shell(App.Path & "\bim " & Combo2.Text & ".a00/oi/nm:100/loop:1", 1)
End Sub

Private Sub Command3_Click()
    Label1 = "fxddxexd"
    Form5.Show

End Sub

Private Sub Command4_Click()
    Form4.Show
```

```
End Sub

Private Sub Command5_Click()
Dim RetVal
   RetVal = Shell("D:\Program Files\HUG\Osiris Version 4.15\Osiris.exe " &
Combo7.Text & ".int", 1)
"\" & Form1.Combo6.Text & ".res"

End Sub

Private Sub Command6_Click()
   Text30.Text = 1
   Text31.Text = 2
   Text32.Text = 3
   Text33.Text = 4

End Sub

Private Sub Form_Load()
Dim FileName As String
Dim Temp As String
Dim X As Integer


   Combo1.AddItem "Rectangular"
   Combo1.AddItem "Ver. Cylindrical"
   Combo1.AddItem "Hor. Cylindrical"
   Combo1.Text = ""

   Combo2.AddItem "Sim1"
   Combo2.AddItem "Sim2"
   Combo2.AddItem "Sim3"
   Combo2.Text = "Sim1"

   Combo3.AddItem "Ellipsoidal"
   Combo3.AddItem "Rectangular"
   Combo3.AddItem "Ver. Cylindrical"
   Combo3.AddItem "Hor. Cylindrical"
   Combo3.AddItem "Point"
   Combo3.Text = ""

   Combo4.AddItem "Triangular"
   Combo4.AddItem "Elliptical"
   Combo4.AddItem "Hexagonal"
   Combo4.AddItem "Rectangular"
   Combo4.Text = ""

   Combo5.AddItem "Parallel-hole"
   Combo5.AddItem "Slant hole"
```

```
Combo5.AddItem "Converging"
Combo5.AddItem "Fan-beam"
Combo5.AddItem "Diverging"
Combo5.Text = ""

Combo6.AddItem "Sim1"
Combo6.AddItem "Sim2"
Combo6.AddItem "Sim3"
Combo6.Text = "Sim1"

Combo7.AddItem "Sim1"
Combo7.AddItem "Sim2"
Combo7.AddItem "Sim3"
Combo7.Text = "Sim1"

Combo8.AddItem "Auto"
Combo8.Text = ""

Combo9.AddItem "Auto"
Combo9.Text = ""

Combo10.AddItem "(57)Co 122 keV"
Combo10.AddItem "(67)Ga 93 keV"
Combo10.AddItem "(99)Tc 140 keV"
Combo10.AddItem "(113)In 392 keV"
Combo10.AddItem "(123)I 159 keV"
Combo10.AddItem "(125)I 35 keV"
Combo10.AddItem "(133)Xn 81 keV"
Combo10.AddItem "(201)Tl 77 keV"
Combo10.Text = ""


FileName = App.Path & "\simind.smc"

Open FileName For Input As #1

X = 1

Do Until EOF(1)
    Line Input #1, Temp

    Select Case X
        Case 2
            Text1.Text = Trim(Left(Temp, 11))
            Temp = Mid(Temp, 12, Len(Temp))
            Text2.Text = Trim(Left(Temp, 11))
            Temp = Mid(Temp, 12, Len(Temp))
            Text3.Text = Trim(Left(Temp, 11))
            Temp = Mid(Temp, 12, Len(Temp))
```

```
        Text4.Text = Trim(Left(Temp, 11))
        Temp = Mid(Temp, 12, Len(Temp))
        Text5.Text = Trim(Left(Temp, 11))
        Temp = Mid(Temp, 12, Len(Temp))
        Text6.Text = Trim(Left(Temp, 9))
        Temp = Mid(Temp, 10, Len(Temp))
        Text7.Text = Trim(Left(Temp, 11))
        Temp = Mid(Temp, 12, Len(Temp))
        Text8.Text = Trim(Left(Temp, 11))
    Case 4
        For Y = 0 To 14
            'If Not y = 1 Then
                Check1(Y).Value = IIf(Mid(Temp, (Y * 2) + 1, 2) = " T", 1, 0)
            'End If
        Next
    Case 6
        'Text9.Text = Trim(Left(Temp, 12))
        Select Case Int(Trim(Left(Temp, 12)))
            Case 35
                Combo10.Text = "(125)I 35 keV"
            Case 77
                Combo10.Text = "(201)Tl 77 keV"
            Case 81
                Combo10.Text = "(133)Xn 81 keV"
            Case 93
                Combo10.Text = "(67)Ga 93 keV"
            Case 122
                Combo10.Text = "(57)Co 122 keV"
            Case 140
                Combo10.Text = "(99)Tc 140 keV"
            Case 159
                Combo10.Text = "(123)I 159 keV"
            Case 392
                Combo10.Text = "(113)In 392 keV"
            Case Else
                Combo10.Text = Trim(Left(Temp, 12))
        End Select
                Temp = Mid(Temp, 13, Len(Temp))
        Text10.Text = Trim(Left(Temp, 12))
        Temp = Mid(Temp, 13, Len(Temp))
        Text11.Text = Trim(Left(Temp, 12))
        Temp = Mid(Temp, 13, Len(Temp))
        Text12.Text = Trim(Left(Temp, 12))
        Temp = Mid(Temp, 13, Len(Temp))
        Text13.Text = Trim(Left(Temp, 12))
    Case 7
        Text14.Text = Trim(Left(Temp, 12))
        Temp = Mid(Temp, 13, Len(Temp))
        Text15.Text = Trim(Left(Temp, 12))
```

```
      Temp = Mid(Temp, 13, Len(Temp))
      Text16.Text = Trim(Left(Temp, 12))
      Temp = Mid(Temp, 13, Len(Temp))
      Text17.Text = Trim(Left(Temp, 12))
      Temp = Mid(Temp, 13, Len(Temp))
      Text18.Text = Trim(Left(Temp, 12))
   Case 8
      Temp = Mid(Temp, 13, Len(Temp))
      Text19.Text = 0 - Trim(Left(Temp, 12))
      Temp = Mid(Temp, 13, Len(Temp))
      Temp = Mid(Temp, 13, Len(Temp))
      'Text20.Text = Trim(Left(Temp, 12))
      Select Case Int(Trim(Left(Temp, 12)))
         Case 2
            Combo1.Text = "Rectangular"
         Case 3
            Combo1.Text = "Ver. Cylindrical"
         Case 4
            Combo1.Text = "Hor. Cylindrical"
         Case Else
            Combo1.Text = Trim(Left(Temp, 12))
      End Select
      Temp = Mid(Temp, 13, Len(Temp))
      'Text21.Text = Trim(Left(Temp, 12))
      Select Case Int(Trim(Left(Temp, 12)))
         Case 1
            Combo3.Text = "Ellipsoidal"
         Case 2
            Combo3.Text = "Rectangular"
         Case 3
            Combo3.Text = "Ver. Cylindrical"
         Case 4
            Combo3.Text = "Hor. Cylindrical"
         Case 5
            Combo3.Text = "Point"
         Case Else
            Combo3.Text = Trim(Left(Temp, 12))
      End Select
   Case 9
      Temp = Mid(Temp, 13, Len(Temp))
      Temp = Mid(Temp, 13, Len(Temp))
      Temp = Mid(Temp, 13, Len(Temp))
      Text22.Text = Trim(Left(Temp, 12))
      Temp = Mid(Temp, 13, Len(Temp))
      'Text23.Text = Trim(Left(Temp, 12))
      Select Case Int(Trim(Left(Temp, 12)))
         Case -20
            Combo8.Text = "Auto"
         Case Else
```

```
         Combo8.Text = Trim(Left(Temp, 12))
      End Select

   Case 10
      'Text24.Text = Trim(Left(Temp, 12))
      Select Case Int(Trim(Left(Temp, 12)))
         Case -20
            Combo9.Text = "Auto"
         Case Else
            Combo9.Text = Trim(Left(Temp, 12))
      End Select
      Temp = Mid(Temp, 13, Len(Temp))
      Text38.Text = Trim(Left(Temp, 12))
      Temp = Mid(Temp, 13, Len(Temp))
      Text39.Text = Trim(Left(Temp, 12))
      Temp = Mid(Temp, 13, Len(Temp))
      Text40.Text = Trim(Left(Temp, 12))
      Temp = Mid(Temp, 13, Len(Temp))
      Text41.Text = Trim(Left(Temp, 12))
   Case 11
      Text25.Text = Trim(Left(Temp, 12))
      Temp = Mid(Temp, 13, Len(Temp))
      Temp = Mid(Temp, 13, Len(Temp))
      Text26.Text = Trim(Left(Temp, 12))
      Temp = Mid(Temp, 13, Len(Temp))
      Text27.Text = Trim(Left(Temp, 12))
      Temp = Mid(Temp, 13, Len(Temp))
      Text28.Text = Trim(Left(Temp, 12))
   Case 15
      Text29.Text = Trim(Left(Temp, 12))
      Temp = Mid(Temp, 13, Len(Temp))
      Text30.Text = Trim(Left(Temp, 12))
      Temp = Mid(Temp, 13, Len(Temp))
      Text31.Text = Trim(Left(Temp, 12))
      Temp = Mid(Temp, 13, Len(Temp))
      Text32.Text = Trim(Left(Temp, 12))
   Case 16
      Temp = Mid(Temp, 13, Len(Temp))
      Text33.Text = Trim(Left(Temp, 12))
      Temp = Mid(Temp, 13, Len(Temp))
      Temp = Mid(Temp, 13, Len(Temp))
      'Text34.Text = Trim(Left(Temp, 12))
      Select Case Int(Trim(Left(Temp, 12)))
         Case 1
            Combo4.Text = "Triangular"
         Case 2
            Combo4.Text = "Elliptical"
         Case 3
            Combo4.Text = "Hexagonal"
```

```
        Case 4
            Combo4.Text = "Rectangular"
        Case Else
            Combo4.Text = Trim(Left(Temp, 12))
        End Select

        Temp = Mid(Temp, 13, Len(Temp))
        'Text35.Text = Trim(Left(Temp, 12))
        Select Case Int(Trim(Left(Temp, 12)))
            Case 0
                Combo5.Text = "Parallel-hole"
            Case 1
                Combo5.Text = "Slant hole"
            Case 2
                Combo5.Text = "Converging"
            Case 3
                Combo5.Text = "Fan-beam"
            Case 4
                Combo5.Text = "Diverging"
            Case Else
                Combo5.Text = Trim(Left(Temp, 12))
        End Select

    Case 21
        Text36.Text = Trim(Left(Temp, 12))
        Temp = Mid(Temp, 13, Len(Temp))
        Text37.Text = Trim(Left(Temp, 12))
    End Select

    X = X + 1
Loop

Close
End Sub

Private Sub Picture1_Click()

End Sub



Private Sub Text10_GotFocus()
    Label1 = "The x dimension of the standard source shape. The value entered is half of the
total dimension."
End Sub

Private Sub Text11_GotFocus()
    Label1 = "The y dimension of the standard source shape. The value entered is half of the
total dimension."
End Sub
```

```
Private Sub Text12_GotFocus()
    Label1 = "The z dimension of the standard source shape. The value entered is half of the
total dimension."
End Sub


Private Sub Text13_GotFocus()
    Label1 = "The x dimension of the standard phantom. The value entered is half of the
total dimension."
End Sub


Private Sub Text14_GotFocus()
    Label1 = "The y dimension of the standard phantom. The value entered is half of the
total dimension."
End Sub


Private Sub Text15_GotFocus()
    Label1 = "The z dimension of the standard phantom. The value entered is half of the
total dimension."
End Sub


Private Sub Text16_GotFocus()
    Label1 = "The length of cylindrical crystal in x-direction. If 'Crystal Half Width' is equal
to zero, then the detector is assumed to be a cylinder, and the radius of the cylinder is
defined by this parameter. [cm]"
End Sub


Private Sub Text17_GotFocus()
    Label1 = "The thickness of the scintillation crystal. [cm]"
End Sub


Private Sub Text18_GotFocus()
    Label1 = "The width of the detector. If this option is equal to zero, than the detector is
assumed to be a cylinder with a radius equal to 'Crystal Half Length/radius'. [cm]"
End Sub


Private Sub Text19_GotFocus()
    Label1 = "The distance from the origin of the coordinate system to the lowest part of the
detector, cm"
End Sub


Private Sub Text25_GotFocus()
Label1 = "This option represents the number of photon histories that are simulated. The
value is given as the number of thousands of histories"
End Sub


Private Sub Text29_GotFocus()
    Label1 = "The length of the collimator hole in the x-direction [cm]"
End Sub
```

```
Private Sub Text30_GotFocus()
    Label1 = "The length of the collimator hole in the y-direction. This value is also known
as the inner hole diameter [cm]"
End Sub


Private Sub Text31_GotFocus()
    Label1 = "The distance between two collimator holes in the x-direction. [cm]"
End Sub


Private Sub Text32_GotFocus()
    Label1 = "The distance between two collimator holes in the y-direction. This value is
also known as the septal thickness [cm]"
End Sub


Private Sub Text33_GotFocus()
    Label1 = "The physical thickness of the collimator [cm]"
End Sub


Private Sub Text38_GotFocus()
    Label1 = "The energy resolution of the detector. [%]"
End Sub


Private Sub Text39_GotFocus()
    Label1 = "The instrinsic spatial resolution of the crystal. [cm]"
End Sub


Private Sub Text41_GotFocus()
    Label1 = "The activity of the source. It is used to obtain correct values of the sensitivity
and different calculated count rates. It does not decide the number of photons that are
actually are simulated. [kBq]"
End Sub


Private Sub Text9_GotFocus()
    Label1 = "The energy of the photon is entered here, keV"
End Sub
Private Sub Text26_GotFocus()
    Label1 = "The pixel size is used to define the area on the crystal that is represented by
the image. The image created can be zoomed in or enlarged aritrarily by giving the proper
value of the pixel size. The value must be bigger than zero"
End Sub
Private Sub Timer1_Timer()
    If Combo1.Text = "Rectangular" Then
        Shape1.Visible = True
        Label35 = Text10.Text
    Else
        Shape1.Visible = False
    End If
```

```
If Combo1.Text = "Ver. Cylindrical" Then
   Shape2.Visible = True
   Label35 = Text11.Text & " cm"
Else
   Shape2.Visible = False
End If

If Combo1.Text = "Hor. Cylindrical" Then
   Shape3.Visible = True
   Label35 = Text11.Text & " cm"
Else
   Shape3.Visible = False
End If

If Combo3.Text = "Ellipsoidal" Then
   Shape4.Visible = True
Else
   Shape4.Visible = False
End If

If Combo3.Text = "Rectangular" Then
   Shape5.Visible = True
Else
   Shape5.Visible = False
End If

If Combo3.Text = "Ver. Cylindrical" Then
   Shape6.Visible = True
Else
   Shape6.Visible = False
End If

If Combo3.Text = "Hor. Cylindrical" Then
   Shape7.Visible = True
Else
   Shape7.Visible = False
End If

If Combo3.Text = "Point" Then
   Shape8.Visible = True
Else
   Shape8.Visible = False
End If

End Sub

Form2
Private Sub Form_Load()
Dim FileName As String
```

```
FileName = App.Path & "\" & Form1.Combo6.Text & ".res"

Open FileName For Input As #1

Text1.Text = ""

Do Until EOF(1)
    Line Input #1, Temp
    Text1.Text = Text1.Text & Temp & vbCrLf
Loop

Close
End Sub

Private Sub Form_Resize()
    Text1.Top = 0
    Text1.Left = 0
    Text1.Width = Form2.ScaleWidth
    Text1.Height = Form2.ScaleHeight
End Sub
```

REFERENCES

1. Cho, Z.H., J.P. Jones, M. Singh, *Foundations of medical imaging*, Wiley-Interscience, New York, 1993.

2. Sprawls, P., *Physical Principles of Medical Imaging*, Aspen Publications, Maryland, 1987.

3. Barnett, H.H., W. Swindell, *Radiological Imaging: The Theory of Image Formation, Detection, and Processing Volume 1*, Academic Press, New York, 1981.

4. Shung, K.K., M.B. Smith, B.M.W. Tsui, *Principles of Medical Imaging*, Academic Press, California, 1992.

5. Nudelman, S., D.D. Patton, *Imaging for Medicine Volume 1*, Plenum Press, New York, 1980.

6. Kalos, M.H., P.A. Whitlock, *Monte Carlo Methods Volume 1: Basics*, Wiley-Interscience, New York, 1986.

7. Morin, Richard L., *Monte Carlo Simulation in the Radiological Sciences*, CRC Press, Florida, 1988.

8. Mettler, F.A., M.J. Guibertaeau, *Essentials of nuclear medicine imaging*, W.B. Saunders, Pennsylvania, 1998.

9. Zaidi, H., "Relevance of accurate Monte Carlo modeling in nuclear medical imaging," *Med. Phys.*, vol. 26, no. 4, pp. 574-608, April 1999.

10. Ljungberg, M., S-E. Strand, M.A. King, *Monte Carlo Calculations in Nuclear Medicine: Applications in Diagnostic Imaging*, IOP, London, 1998.

11. Ljungberg, M., "Development and Evaluation of Attenuation and Scatter Correction Techniques for SPECT Using The Monte Carlo Method," Ph.D. Dissertation, University of Lund, 1990.

12. Anger, H.O. "Scintillation Camera," *Rev. Sci. Instrum.*, vol. 35, pp. 27-33, 1958.

13. Evans, R.D. *The Atomic Nucleus*, McGraw-Hill, New York, 1955.

14. URL: hhtp://www.nuclearfield.com

15. URL: http://www.geocities.com/CollegePark/Quad/2435

16. Marsaglia, G., A. Zaman, "Monkey Tests for Random Number Generators," *Comput. Math. Appl.*, vol. 23, pp. 1-10, 1993.

17. Anderson, S. L., "Random Number Generators on Vector Supercomputers and Other Advanced Architectures," *SIAM (Soc. Ind. Appl. Math.)*, vol. 32, pp. 221-251, 1990.

18. Marsaglia, G., and A. Zaman, "Some Portable Very-Long-Period Random Number Generators," *Comput. Phys.*, vol. 8, pp. 117-121, 1994.

19. Bielajew, A. F., D.W.O. Rogers, *"Variance-Reduction Techniques,"* in T. Jenkins, W. Nelson, A. Rindi, A. Nahum, and D. Rogers (Eds.), *Monte Carlo Transport of Electrons and Photons,* pp. 407-419, Plenum, New York, 1989.

20. Haynor, D. R., R. L. Harrison, and T. K. Lewellen, "Improving The Efficiency of Emission Tomography Using Variance Reduction Techniques," *IEEE Trans. Nucl. Sci.*, vol. 37, pp. 749-753, 1990.

21. Zubal, I. G., C. R. Harell. "Voxel-Based Monte Carlo Calculations of Nuclear Medicine Images and Applied Variance Reduction Techniques," *Image Vis. Comput.*, vol. 10, pp. 342-348, 1992.

22. Gantet, P., J. P. Esquerre, B. Danet, and R. Guiraud, "A Simulation Method for Studying Scintillation Camera Collimators," *Phys. Med. Biol.*, vol. 35, pp. 659-669, 1990.

23. Webb S., D. M. Binnie, M. A. Flower, and R. J. Ott, "Monte Carlo Modeling of The Performance of A Rotating Slit-Collimator for Improved Planar Gamma-Camera Imaging," *Phys. Med. Biol.*, vol. 37, pp. 1095-1108, 1992.

24. Moore, S. C., D. J. de Vries, B. Nandram, M. F. Rijewski, and S. P. Mueller, "Collimator Optimization for Lesion Detection Incorporating Prior Information About Lesion Size," *Med. Phys.*, vol. 22, pp. 703-713, 1995.

25. Kojima, A., M. Matsumoto, M. Takahashi, and S. Uehara, "Effect of Energy Resolution on Scatter Fraction in Scintigraphic Imaging: Monte Carlo Study," *Med. Phys.*, vol. *20*, pp. 1107-1113, 1993.

26. Andreo, P., "Monte Carlo Techniques in Medical Radiation Physics," *Phys. Med. Biol.*, vol. 36, pp. 861-920, 1991.

27. Ogawa, K., S. Takahashi, and Y. Satori, "Description of an Object in Monte Carlo Simulations," IEEE *Trans. Nucl. Sci.*, vol. 44, pp. 1521-1526, 1997.

28. Wang. H., R. J. Jaszczak, R. E. Coleman, "Solid Geometry-Based Object Model for Monte Carlo Simulated Emission and Transmission Tomographic Imaging Systems," *IEEE Trans. Med. Imaging*, vol.11, pp. 361-372, 1992.

29. LaCroix, K. J., "Evaluation of An Attenuation Compensation Method With Respect to Defect Detection in Tc-99m-Sestamibi Myocardial SPECT," Ph.D. Dissertation, The University of North Carolina at Chapel Hill, Chapel Hill, NC, 1997.

30. Nelson, W. R., H. Hirayama, D. W. O. Rogers, "The EGS4 Code System," SLAC-256, Stanford Linear Accelerator Center, Stanford, CA, 1985.

31. Halbleib, J. A., R. P. Kensek, G. D. Valdez, S. M. Seltzer, and M. J. Berger, "ITS: The Integrated TIGER Series Of Electron/Photon Transport Codes-Version 3.0," *IEEE Trans. Nucl. Sci.*, vol. 39, pp. 1025-1030, 1992.

32. Briesmeister, J. F., "MCNP - A General Monte Carlo Code For Neutron And Photon Transport," Version 3A, Los Alamos, NM, Los Alamos National Laboratory, LA-12625-M, 1997.

33. Harrison, R. L., S. D. Vannoy, D. R. Haynor, S. B. Gillispie, M. S. Kaplan, and T. K. Lewellen, "Preliminary Experience with the Photon History Generator Module for A Public-Domain Simulation System for Emission Tomography," *Conf. Rec. IEEE Med. Imag. Conf.,* San Francisco, 1993, pp. 1154-1158, New York, IEEE, 1994.

34. Ljungberg, M., Strand, S-E., "A Monte Carlo Program for the Simulation of Scintillation Camera Characteristics," Computer Programs and Methods in Biomedicine., vol. 29, pp. 257-272, 1989.

35. Smith, M. F., C. E. Floyd, and R. J. Jaszczak, "A Vectorized Monte Carlo Code for Modeling Photon Transport in SPECT," *Med. Phys.*, vol. 20, pp. 1121-1127, 1993.

36. Thompson, C. J., J.M. Cantu, Y. Picard, "PETSIM: Monte Carlo Program Simulation of All Sensitivity and Resolution Parameters of Cylindrical Positron Imaging Systems," *Phys. Med. Biol.*, vol. 37, pp. 731-749, 1992.

37. Ligier Y., O. Ratib, M. Logean, C. Girard, "Osiris: A Medical Image Manipulation System," *Computing Journal*, vol. 11, pp. 212-218, 1994.